



# THE STATE OF THE CLIMATE IN 2016

Ole Humlum

The Global Warming Policy Foundation

GWPF Report 23

## **GWPF REPORTS**

Views expressed in the publications of the Global Warming Policy Foundation are those of the authors, not those of the GWPF, its Academic Advisory Council members or its directors

## **THE GLOBAL WARMING POLICY FOUNDATION**

---

### **Director**

Benny Peiser

### **BOARD OF TRUSTEES**

---

Lord Lawson (Chairman)	Peter Lilley MP
Lord Donoghue	Charles Moore
Lord Fellowes	Baroness Nicholson
Rt Revd Dr Peter Forster, Bishop of Chester	Graham Stringer MP
Sir Martin Jacomb	Lord Turnbull

### **ACADEMIC ADVISORY COUNCIL**

---

Professor Christopher Essex (Chairman)	Professor Ross McKittrick
Sir Samuel Brittan	Professor Garth Paltridge
Sir Ian Byatt	Professor Ian Plimer
Dr John Constable	Professor Paul Reiter
Professor Vincent Courtillot	Dr Matt Ridley
Professor Freeman Dyson	Sir Alan Rudge
Christian Gerondeau	Professor Nir Shaviv
Dr Indur Goklany	Professor Philip Stott
Professor William Happer	Professor Henrik Svensmark
Professor David Henderson	Professor Richard Tol
Professor Terence Kealey	Professor Anastasios Tsonis
Professor Deepak Lal	Professor Fritz Vahrenholt
Professor Richard Lindzen	Dr David Whitehouse
Professor Robert Mendelsohn	

### **CREDITS**

---

Cover image NASA  
Public domain

# **THE STATE OF THE CLIMATE IN 2016**

Ole Humlum

ISBN 978-0-9931189-4-4

© Copyright 2017 The Global Warming Policy Foundation



# Contents

About the author	vii
Executive summary	ix
1 General overview 2016	1
2 The spatial pattern of global surface air temperatures in 2016	3
3 Global monthly lower troposphere air temperatures since 1979	5
4 Global mean annual lower troposphere air temperatures since 1979	7
5 Global monthly surface air temperatures since 1979	8
6 Global mean annual surface air temperature since 1850	10
7 Comparing surface air temperatures with temperatures recorded by satellites	11
8 Global monthly lower troposphere air temperatures since 1979; oceans versus land	12
9 Atmospheric temperatures from the surface to 17 km altitude	13
10 Atmospheric greenhouse gases: water vapour and carbon dioxide	14
11 Zonal surface air temperatures	16
12 Polar air temperatures	17
13 Sea surface temperature anomaly at the end of 2015 and 2016	18
14 Global ocean average temperatures to 1900 m depth	20
15 Global ocean temperatures at different depths	21
16 Regional ocean temperature changes at 0–1900 m	23
17 Ocean temperature net change 2004–2016 in two north–south sectors	24
18 Pacific Decadal Oscillation	27

<b>19</b>	<b>Atlantic Multidecadal Oscillation</b>	<b>28</b>
<b>20</b>	<b>Sea level from satellite altimetry</b>	<b>29</b>
<b>21</b>	<b>Sea level from tide gauges</b>	<b>30</b>
<b>22</b>	<b>Annual accumulated cyclone energy for the Atlantic Basin</b>	<b>32</b>
<b>23</b>	<b>Global, Arctic and Antarctic sea-ice extent</b>	<b>33</b>
<b>24</b>	<b>Northern hemisphere snow-cover extent</b>	<b>34</b>
<b>25</b>	<b>Links to data sources</b>	<b>37</b>

## **About the author**

Ole Humlum is Professor of Physical Geography at the University Centre in Svalbard, Norway.



## Executive summary

1. It is likely that 2016 was one of the warmest years in the temperature records from the instrumental period (since about 1850). However, by the end of 2016, global air temperatures were essentially back to the level of the years before the recent 2015–16 oceanographic El Niño episode, although there are small differences between the individual temperature records. This fact reveals that the global 2015–16 surface temperature peak was caused mainly by El Niño. It also suggests that what has been termed the ‘hiatus’, ‘pause’ or ‘period of gentle warming’ may endure after the recent El Niño episode.
2. There appears to be a systematic difference developing between global air temperatures as estimated by surface stations and by satellites. Especially since 2003, the global temperature estimate based on surface station measurements has consistently drifted away from the satellite-based estimate in a warm direction, and is now about 0.1°C higher.
3. The temperature variations recorded in the lower troposphere are generally reflected at higher altitudes too, and the overall temperature ‘pause’ since about year 2002 is recorded at all altitudes, including the tropopause and into the stratosphere. In the stratosphere, however, the temperature ‘pause’ began as early as around 1995; that is, 5–7 years before a similar temperature ‘pause’ began in the lower troposphere near the Earth’s surface. The stratospheric temperature ‘pause’ has now endured without interruption for about 22 years.
4. The recent 2015–16 oceanographic El Niño is among the strongest since the beginning of the record in 1950. Considering the entire record, however, recent variations of El Niño and La Niña episodes do not appear to deviate from the previous pattern.
5. Much of the heat given off during the 2015–16 El Niño appears to have been transported to the polar regions, especially to the Arctic, causing severe weather phenomena and unseasonably high air temperatures. Subsequently, the heat may have been radiated out to space, as latitudes north of 70°N have been characterised by above-normal outgoing longwave radiation during the northern hemisphere autumn and early winter of 2016.
6. Since 2004, when the Argo buoys came into operation, the global oceans above 1900 m depth have, on average, warmed somewhat. The maximum warming (from the surface to about 120 m) affects the oceans near the Equator, and surface warming is absent or small at higher latitudes in both hemispheres. The maximum ocean surface warming has taken place at latitudes where the incoming solar radiation is at its annual maximum. Net cooling since 2004 is pronounced for the North Atlantic.

7. Data from tide gauges all over the world suggest an average global sea-level rise of 1–1.5 mm/year, while the satellite-derived record suggests a rise of more than 3 mm/yr. The noticeable difference between the two data sets still has no broadly accepted explanation.
8. Arctic and Antarctic sea-ice extents since 1979 have developed in opposite directions, decreasing and increasing, respectively. Superimposed on these overall trends, shorter variations are also important to understand year-to-year variations. In the Arctic, a 5.3-year periodic variation is important, while for the Antarctic a cycle of about 4.5 years duration is important. Both these variations reached their minima simultaneously in 2016, which explains the recent minimum in global sea-ice extent.
9. The northern hemisphere snow-cover extent has important local and regional variations from year to year. The overall tendency (since 1972), however, is a stable overall snow extent.

# 1 General overview 2016

The year 2016 was affected by the oceanographic phenomenon El Niño in the Pacific Ocean. It is likely that 2016 was one of the warmest years in the longest global air temperature record (HadCRUT), which extends back to 1850. However, by the end of 2016, global air temperatures were again back to the level of the years before the recent El Niño episode, suggesting that the global 2015–16 surface temperature peak was caused mainly by this oceanographic phenomenon.

Many diagrams in this report focus on the period from 1979 onwards. This represents the start of the satellite era, from when access to a wide range of observations with nearly global coverage, including temperature, became available. These data provide a detailed view of temperature changes over time at different altitudes in the atmosphere. Among other phenomena, these observations reveal that while the well-known lower-troposphere temperature pause began around 2002, a similar stratospheric temperature plateau had already started already by 1995, several years before the similar temperature plateau near the Earth's surface. Until now, little attention has been paid to this aspect of global climate change.

Surface air temperatures are understandably at the core of the climate debate, but the significance of any short-term warming or cooling in surface air temperatures should not be overstated. Whenever the Earth experiences a warm El Niño or a cold La Niña episode, major heat exchanges take place between the Pacific Ocean and the atmosphere above, eventually showing up as a signal in estimates of the global air temperature. However, this does not reflect a similar change in the total heat content of the atmosphere–ocean system. In fact, global net changes may be small, and such heat exchanges may mainly reflect a redistribution of energy between the ocean and atmosphere. Evaluating the dynamics of ocean temperatures is therefore just as important as evaluating changes of surface air temperatures.

Since 2004 the 3800 Argo floats have provided a unique ocean temperature data set for depths down to 1900 m. Although the oceans are much deeper than 1900 m, and the Argo data series is still relatively short, several interesting features are now emerging from these empirical observations.

Globally since 2004, the upper 1900 m of the oceans have been warming on average change. The maximum warming affects the top 100 m, especially near the Equator. At about 200 m depth, cooling has on average taken place. At greater depths, some net warming has occurred since 2004.

This global average oceanic change since 2004 is reflected in Equatorial oceans between 30°N and 30°S, representing a huge surface area. At the same time, the northern oceans (55–65°N) have on average experienced a marked cooling down to 1300 m depth, and some warming at greater depths. The southern oceans (55–65°S) have on average seen slight warming at all depths since 2004. However, as is well known, averages may be misleading, and quite often a better insight is obtained by

studying the details.

Air-temperature data suggests that a part of the heat released from the Pacific Ocean during the recent El Niño episode may have been transported towards the polar regions, especially in the northern hemisphere, mainly via the Atlantic sector. Many Arctic regions experienced high temperatures in 2016, especially in the autumn and early winter, along with associated weather-related phenomena. At the same time, north of 70°N, the outgoing longwave radiation from the top of the atmosphere has been above normal. Through this mechanism, much of the additional heat released to the atmosphere from the Pacific Ocean may have been lost to space from the Arctic region.

A fascinating difference is developing between global air temperatures estimated by surface stations (HadCRUT, NCDC and GISS)<sup>†</sup> and by satellites (UAH and RSS),<sup>‡</sup> respectively. In the early part of the temperature record after 1979, the satellite-based temperatures were often – but not always – somewhat higher than the temperatures estimated from surface observations. Since 2003, however, the temperature estimate from the surface stations has consistently drifted away from the satellite-based estimates in a warm direction, and is now on average about 0.1 °C higher.

At the end of 2016, the global sea-ice extent reached a marked minimum. This was at least partly caused by the operation of two different natural cycles of the sea ice in the northern and the southern hemispheres. In 2016, both cycles had simultaneous minima, with inevitable consequences for global sea-ice extent. It is therefore likely that coming years will be characterised by somewhat different changes in global sea-ice extent.

Variations in global snow-cover extent are mainly caused by changes in the northern hemisphere, where most of the major land masses are located. The southern hemisphere snow-cover extent is essentially controlled by the Antarctic ice sheet, and is therefore relatively stable. The northern hemisphere average snow cover extent has also been stable since the onset of satellite observations, although local and regional interannual variations may be large. Considering seasonal changes, the northern hemisphere autumn snow-cover extent is increasing a little, the mid-winter extent is largely stable, and the spring extent is declining a little.

Global sea levels are monitored by satellite altimetry and by direct measurements from tide gauges. While the satellite-derived record suggests a global sea-level rise of more than 3 mm per year, data from tide gauges all over the world suggest a stable, average global sea-level rise of less than 1.5 mm per year. The marked difference between the two datasets still has no broadly accepted explanation. What remains sig-

---

<sup>†</sup> HadCRUT is a cooperative effort between the Hadley Centre for Climate Prediction and Research and the University of East Anglia's Climatic Research Unit (CRU), UK. NCDC is the National Climatic Data Center, USA. GISS is the Goddard Institute for Space Studies, USA.

<sup>‡</sup> UAH is the University of Alabama at Huntsville. RSS is Remote Sensing Systems Inc.

nificant, however, is that for local coastal planning the tide-gauge data are the more important, as is explained later.

## 2 The spatial pattern of global surface air temperatures in 2016

On average, the global surface air temperature for 2016 was above the average of the past ten years, as was the case in 2015. Both 2015 and 2016 were affected by the recent El Niño episode in the Pacific Ocean, which peaked in early 2016.

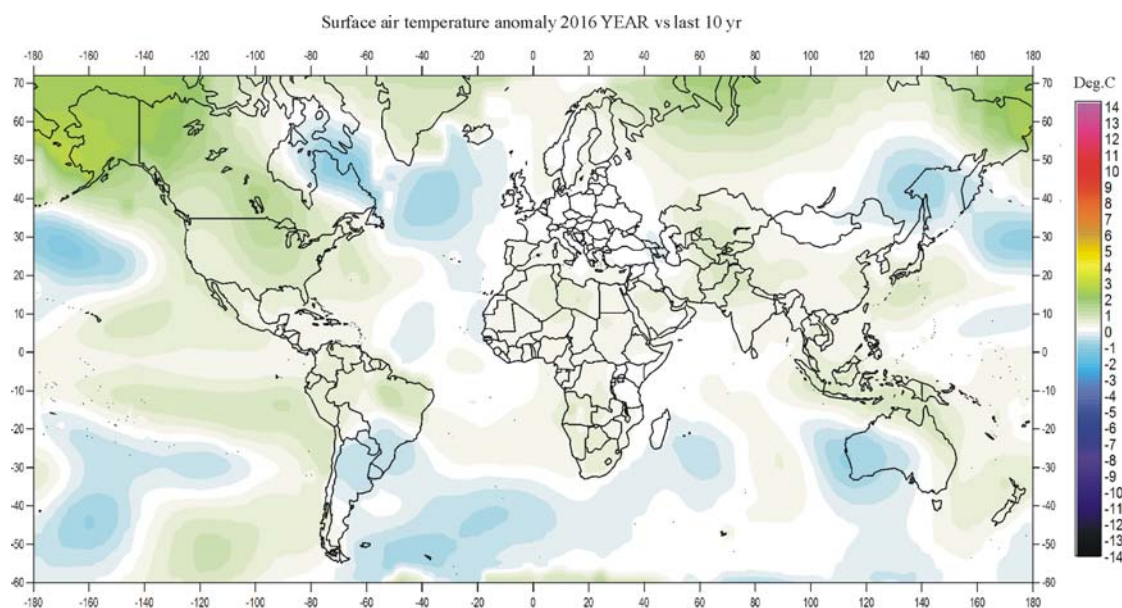


Figure 1: 2016 surface air temperatures compared to the average for the previous ten years.

Green-yellow-red colours indicate areas with higher temperatures than the average, while blue colours indicate lower-than-average temperatures. Data source: GISS.

The northern hemisphere was characterised by regional temperature contrasts, but was generally warm north of 60°N. Alaska and the Arctic Ocean in particular were warm. Relatively cold regions were only found in parts of the North Atlantic and in the Pacific Ocean. Most of North America had above-average temperatures, Europe was close to the average, and most of Russia, Siberia, and Asia were somewhat above average.

Near the Equator, temperatures were generally near the average of the previous ten years. In the Pacific, however, temperatures were relatively high, reflecting the El Niño, which was still playing out during the first part of 2016.

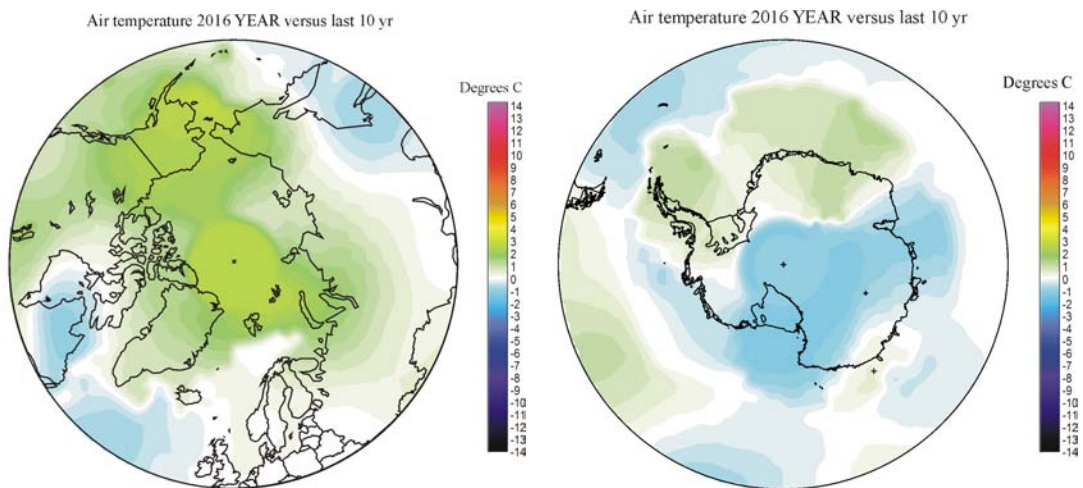


Figure 2: 2016 polar surface air temperatures compared to the average for the previous ten years.

Green-yellow-red colours indicate areas with higher temperature than the average, while blue colours indicate lower-than-average temperatures. Data source: GISS.

In the southern hemisphere, surface air temperatures were near or below the average for the previous ten years. In particular, western Australia and central South America had average temperatures somewhat below the average.

In the Arctic, most regions in 2016 had above-average temperatures, especially within the Alaska and Greenland sectors of the Arctic. The temperature pattern for 2016 is, however, influenced by what is probably an interpolation error at GISS, which results in an implausible circular temperature plateau north of 80°N.

The Antarctic continent was divided into regions with above- and below-average temperatures in 2016, in contrast to 2015, where the entire continent was characterised by below-average temperatures. Another probable interpolation error appears to influence the pattern south of 80°S as well.

Globally speaking, at the end of 2016, air temperatures were essentially back to the level normal in the years leading up to the recent 2015–16 El Niño. Thus the global surface air temperature peak of 2015–16 appears to be mainly caused by this oceanographic phenomenon.

### 3 Global monthly lower troposphere air temperatures since 1979

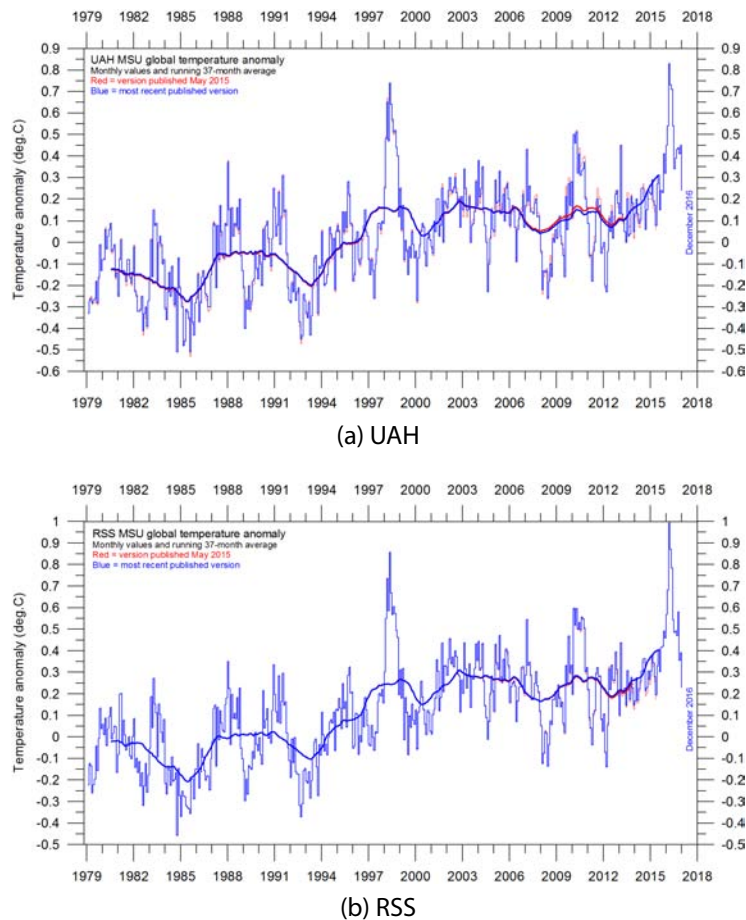
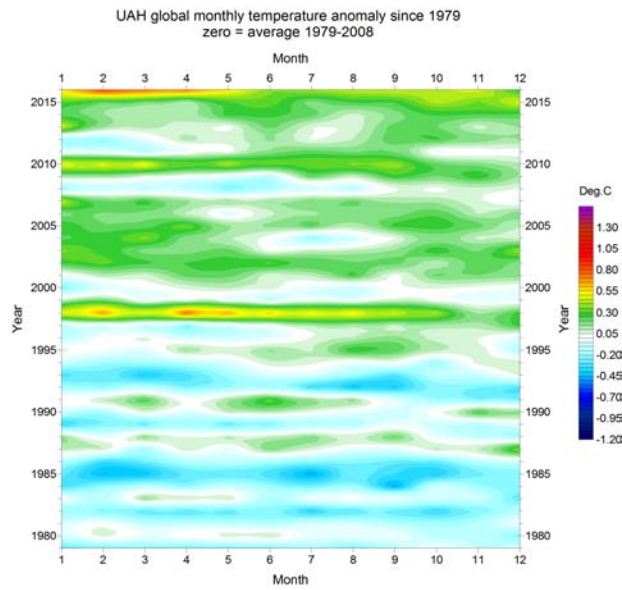


Figure 3: Global monthly average lower troposphere temperatures since 1979, representing conditions at about 2 km altitude.

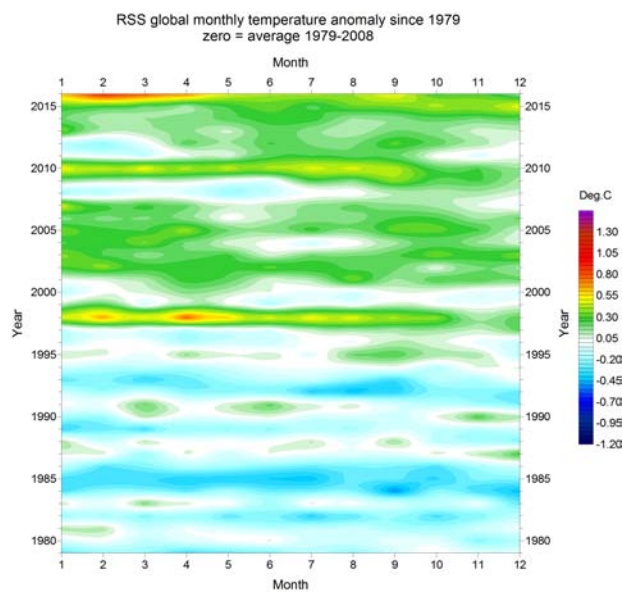
The thick lines are the simple running 37-month average, nearly corresponding to a running 3-yr average.

Both satellite records for the lower troposphere temperature clearly show the temperature spike associated with the 2015–16 El Niño. At the end of 2016, however, the global temperature was back to the general level characterising the period before the recent El Niño. From the two temporal diagrams (Figure 4) the El Niño peak in early 2016 is clearly visible.

The comparison between the latest (December 2016) record and the May 2015 record (red) shows that only a few small adjustments have since been introduced in these two records.



(a) UAH



(b) RSS

Figure 4: Temporal diagrams showing global monthly lower troposphere temperatures since 1979, interpreted by UAH and RSS, respectively.

The effects of the El Niños of 1998, 2010 and 2016 are clearly visible, as is the tendency for many El Niños to peak during the northern hemisphere winter. As the different temperature databases use different reference periods, the series have been made comparable by setting their individual 30-year averages for 1979–2008 at a zero value.

## 4 Global mean annual lower troposphere air temperatures since 1979

Both satellite records show the years 1998 and 2016 to have been similarly warm (Figure 5). Both years were influenced by strong El Niño episodes in the Pacific Ocean.

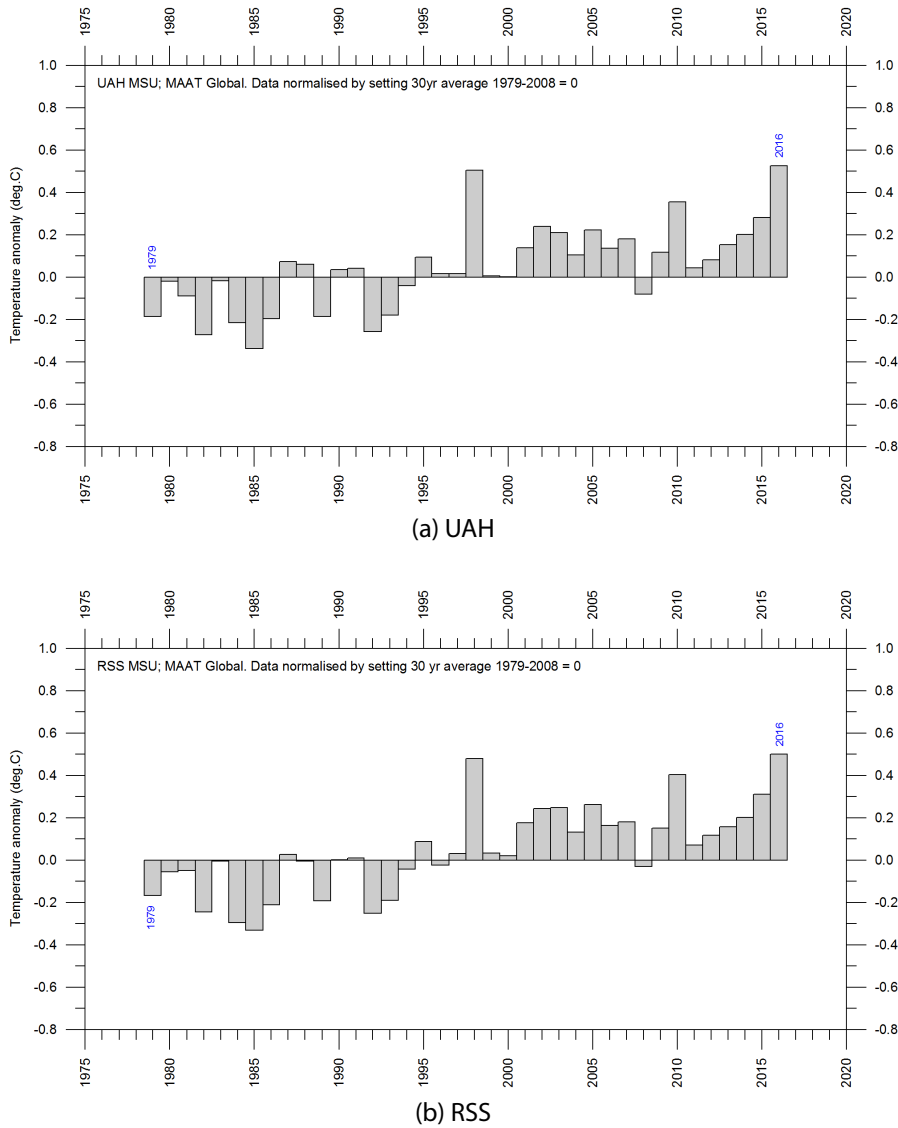


Figure 5: Global mean annual lower troposphere air temperatures since 1979. Satellite data interpreted by UAH and RSS.

## 5 Global monthly surface air temperatures since 1979

All three surface air temperature records clearly show the temperature spike associated with the 2015–16 El Niño. At the end of 2016, however, the global temperature was again approaching the general level characterising the period before the recent El Niño (Figure 6).

The comparison between the most recent (December 2016) record and the May 2015 record (red) shows that few adjustments have since been introduced in the HadCRUT record over the intervening period, while numerous and relatively large changes have been introduced into the NCDC and GISS records. All three surface records, however, confirm that the recent El Niño episode peaked in early 2016 (Figure 7).

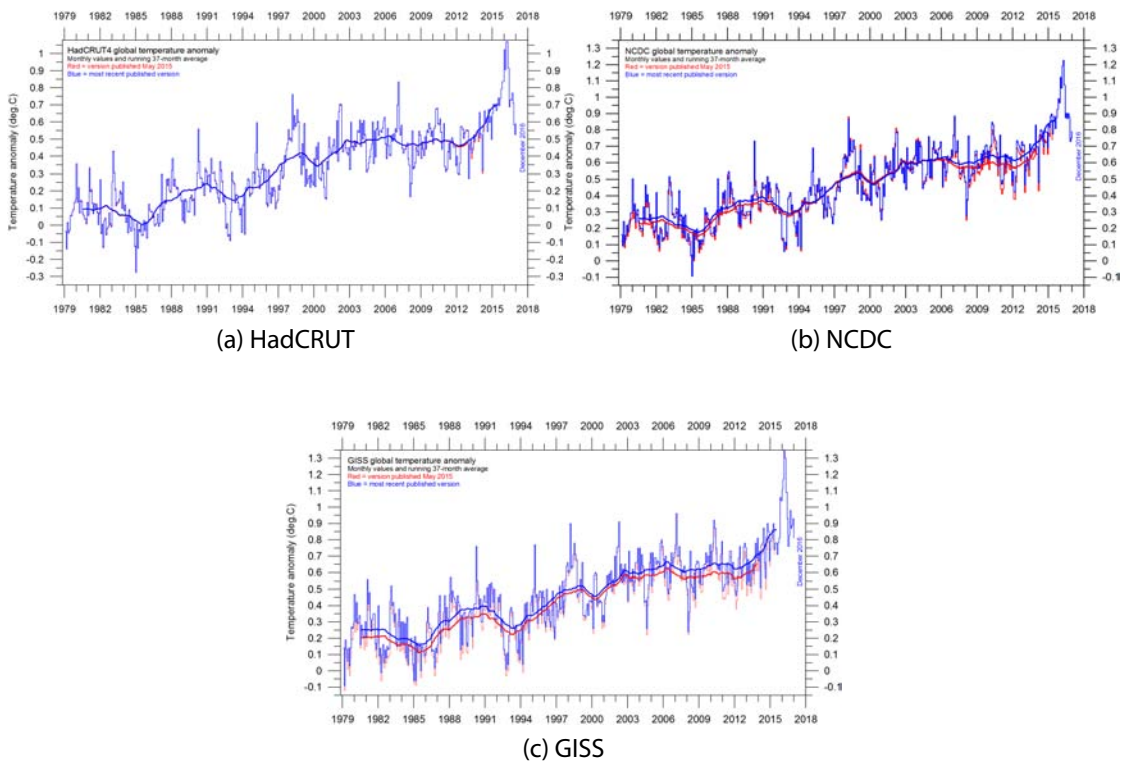
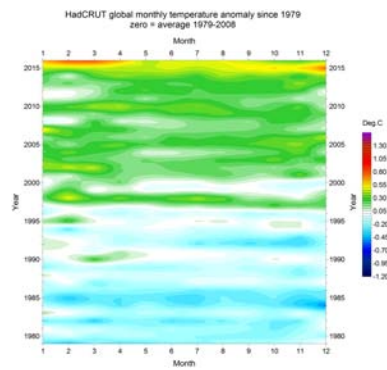
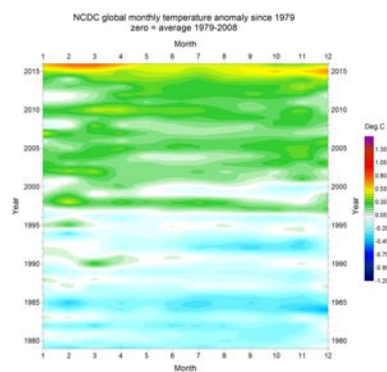


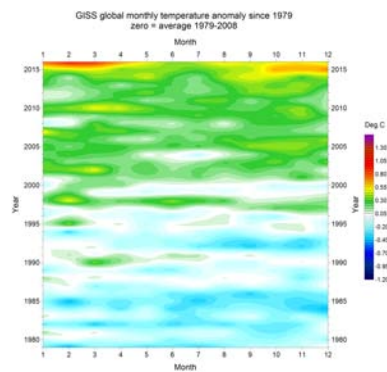
Figure 6: Three records of global monthly average surface air temperatures since 1979. The thick blue line is the simple running 37-month average, nearly corresponding to a running 3-yr average. The red line is the version published in May 2015.



(a) HadCRUT



(b) NCDC



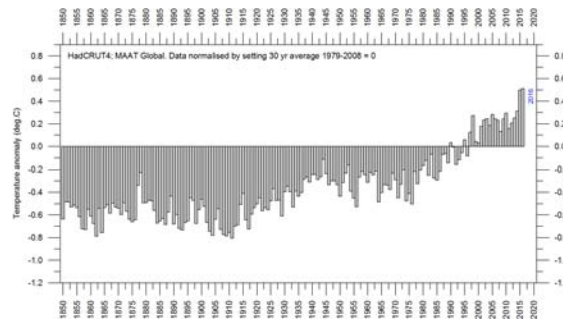
(c) GISS

Figure 7: Temporal diagrams showing global monthly lower troposphere temperatures since 1979, interpreted by HadCRUT, NCDC and GISS.

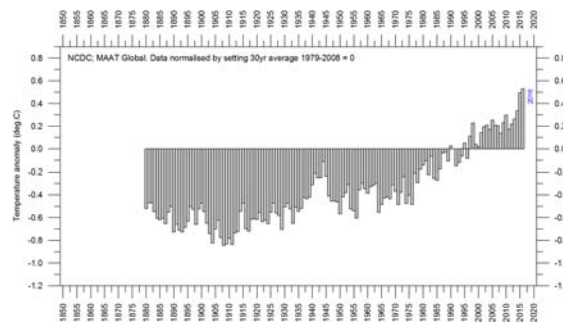
In contrast to the satellite-based diagrams, the effects of the recent 2016 El Niño episode is more pronounced than the El Niños in 1998 and 2010. As the different temperature databases are using different reference periods, the series have been made comparable by setting their individual 30-year average 1979–2008 as zero value.

## 6 Global mean annual surface air temperature since 1850

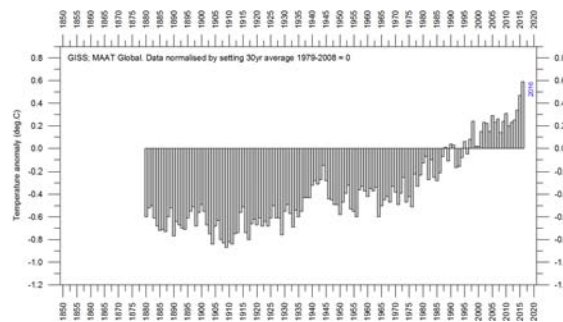
All three surface air temperature estimates show the year 2016 to be the warmest on record. The years 2015 and 2016 were, however, influenced by the recent strong El Niño episode.



(a) HadCRUT



(b) NCDC



(c) GISS

Figure 8: Three records of global mean annual surface air temperatures since 1850 or 1880.

## 7 Comparing surface air temperatures with temperatures recorded by satellites

There is an interesting difference between global air temperatures estimated by surface stations and by satellites (Figure 9). In the early part of the record since 1979, satellite-based temperatures were often somewhat higher than the global estimate derived from surface observations. Since 2003, however, the temperature estimate from the surface stations has consistently drifted away from the satellite-based estimate in a warm direction, and is now about  $0.1^{\circ}\text{C}$  higher.

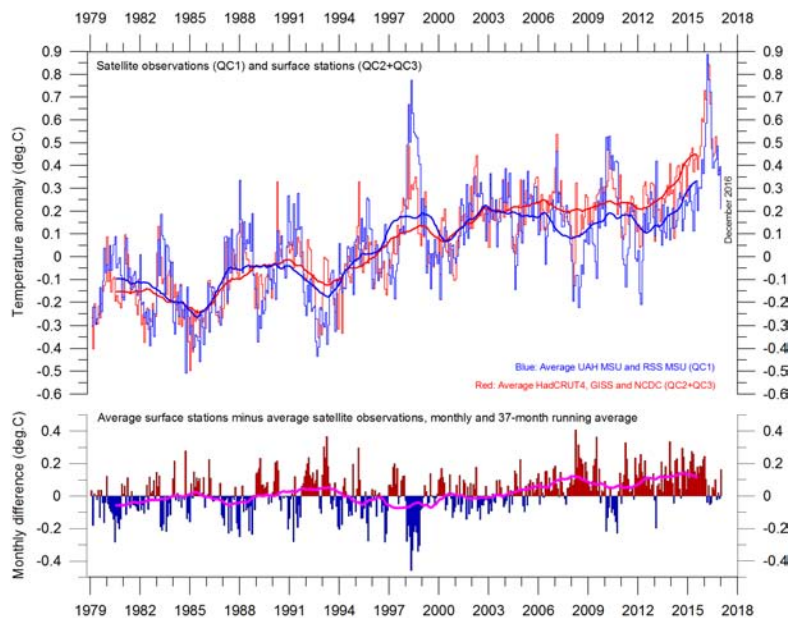


Figure 9: Plot showing the average of monthly global surface air temperature estimates (HadCRUT, NCDC and GISS) and satellite-based temperature estimates (UAH and RSS).

The thin lines indicate the monthly values, while the thick lines represent the simple running 37-month average, nearly corresponding to a running 3-yr average. The lower panel shows the monthly difference between surface air temperatures and satellite temperatures. As the base period differs for the different temperature estimates, they have been normalised on the average value for the 30 years from January 1979 to December 2008.

## 8 Global monthly lower troposphere air temperatures since 1979; oceans versus land

Since 1979, lower troposphere temperatures have increased more over land than over the oceans. In particular, from about 2006 to 2015, temperatures recorded over land were consistently higher than over the oceans. There may be several reasons for this, such as variations in insolation, cloud cover and land use.

This development has apparently taken place roughly at the same time as the drift of surface observations towards higher temperatures relative to satellite-based temperatures.

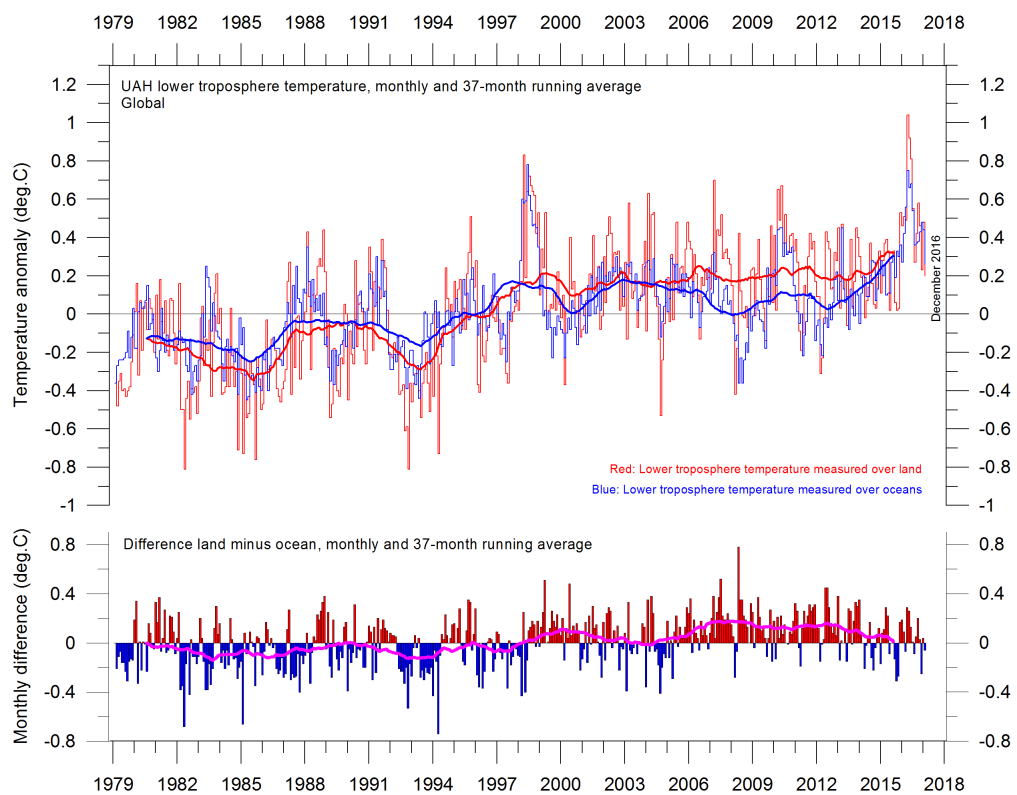


Figure 10: Global monthly average lower troposphere temperature since 1979 measured over land and oceans, according to University of Alabama at Huntsville (UAH), USA.

Red, temperatures over land; blue, temperatures over oceans. The thin lines represent the monthly average, and the thick line the simple running 37-month average, approximately corresponding to a running 3-yr average.

## 9 Atmospheric temperatures from the surface to 17 km altitude

The temperature variations recorded in the lower troposphere are generally reflected at higher altitudes, up to at least 5–6 km altitude. The overall temperature plateau since about 2002 is found at all these altitudes. At higher altitudes, near the tropopause (about 10 km altitude), the pattern of variations recorded lower in the atmosphere can still be seen, but for the duration of the record (since 1979) there has been no trend towards higher or lower temperatures.

Higher in the atmosphere, in the stratosphere at 17 km altitude, two pronounced temperature spikes are visible before the turn of the century. Both spikes are related to major volcanic eruptions, as indicated. Ignoring these spikes, until about 1995 the stratospheric temperature record shows a persistent decline. This has been ascribed by some scientists to the effect of more and more heat being trapped in the troposphere below, due to an increase in CO<sub>2</sub>. However, this temperature decline ends in around 1995–96, and a long temperature plateau has since been observed in the stratosphere. Thus, the stratospheric temperature ‘pause’ began 5–7 years before a similar ‘pause’ was seen in the lower troposphere.

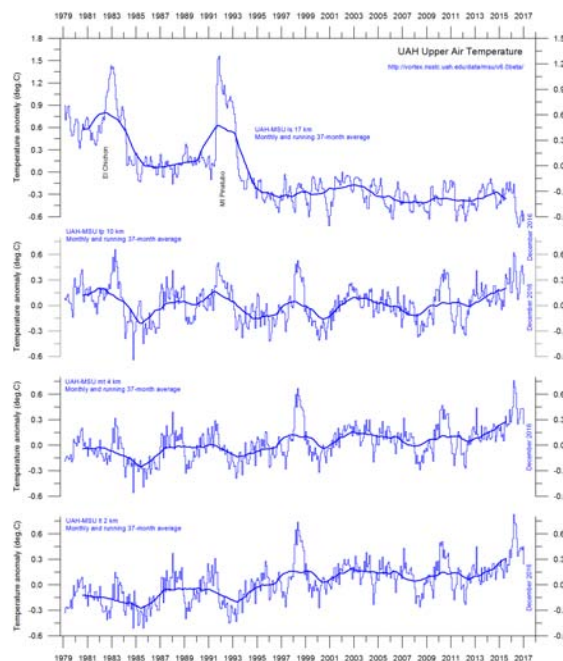


Figure 11: Global monthly average temperature in different altitudes according to University of Alabama at Huntsville (UAH), USA.

The thin lines represent the monthly average, and the thick line the simple running 37-month average, nearly corresponding to a running 3-yr average.

## 10 Atmospheric greenhouse gases: water vapour and carbon dioxide

Water vapour is the most important greenhouse gas in the troposphere. The highest concentration is found in a latitudinal range from 50°N to 60°S. The two polar regions of the troposphere are comparatively dry.

The specific atmospheric humidity is stable or slightly increasing up to about 4–5 km altitude. At higher levels in the troposphere (about 9 km), the specific humidity has been decreasing for the duration of the record (since 1948), but with shorter variations superimposed on this trend. A Fourier frequency analysis (not shown here) shows these variations to be influenced by a periodic variation of about 3.7-years' duration.

The persistent decrease in specific humidity at about 9 km altitude is interesting, as this altitude roughly corresponds to the level where the theoretical temperature effect of atmospheric carbon dioxide is expected to play out initially.

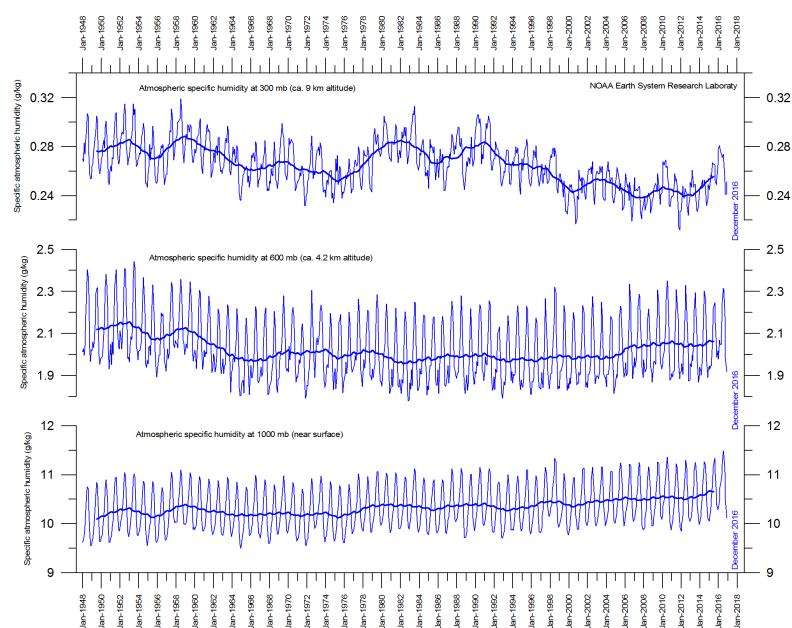
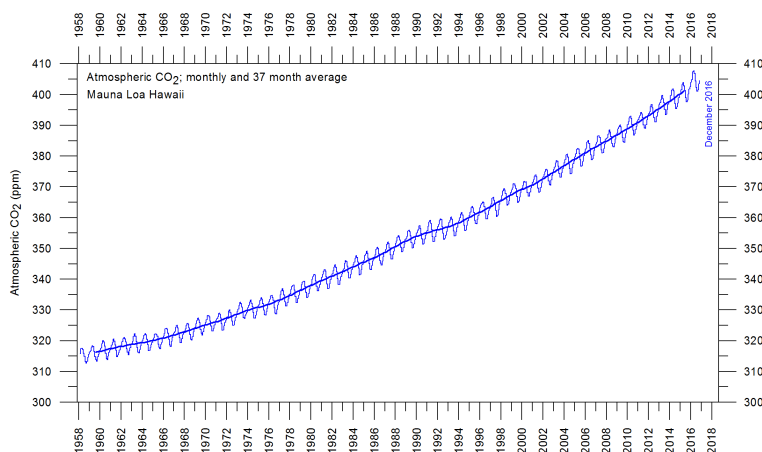


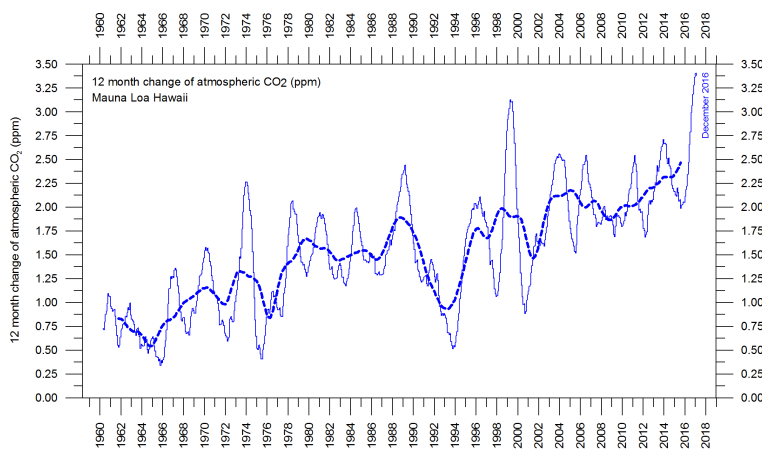
Figure 12: Specific atmospheric humidity (g/kg) at three different altitudes in the troposphere since January 1948.

The thin blue lines show monthly values, while the thick blue lines show the running 37-month average (about 3 years). Source: ERSI.

Carbon dioxide is an important greenhouse gas, although less important than water vapour. For the duration of the Mauna Loa record (since 1958), an increasing trend is clearly visible, with an annual cycle superimposed (Figure 13a). At the end of



(a) Monthly concentrations since March 1958; thin line, monthly values; thick line, simple running 37-month average, nearly corresponding to a running 3-yr average.



(b) Annual growth rate since 1959 (average for current 12 months less average for previous 12 months). Thin line, month-by-month values; dotted line, 3-yr average; ppm, parts per million.

Figure 13: Carbon dioxide concentrations at the Mauna Loa observatory, Hawaii.

2016, the amount of atmospheric carbon dioxide is slightly above 400 parts per million (ppm). Carbon dioxide is normally considered a relatively well-mixed gas in the troposphere.

The 12-month change in tropospheric carbon dioxide levels has been increasing from about +1 ppm/year in the early part of the record to more than +2 ppm/yr towards the end (Figure 13b). A Fourier frequency analysis (not shown here) shows the 12-month change of tropospheric carbon dioxide to be influenced by periodic variations of 2.5 and 3.8 years' duration, respectively.

## 11 Zonal surface air temperatures

Figure 14 shows that the 'global' warming experienced after 1980 was predominantly a northern-hemisphere phenomenon, and mainly took place as a marked change between 1994 and 1999. This apparently rapid temperature change was, however, influenced by the Mount Pinatubo eruption in 1992–93 and the 1997 El Niño episode.

The diagram also shows the temperature effects of the equatorial El Niños in 1997 and 2015–16 spreading over higher latitudes in both hemispheres. The temperature effect was, however, mainly recorded in the northern hemisphere, and only to lesser degree in the southern hemisphere.

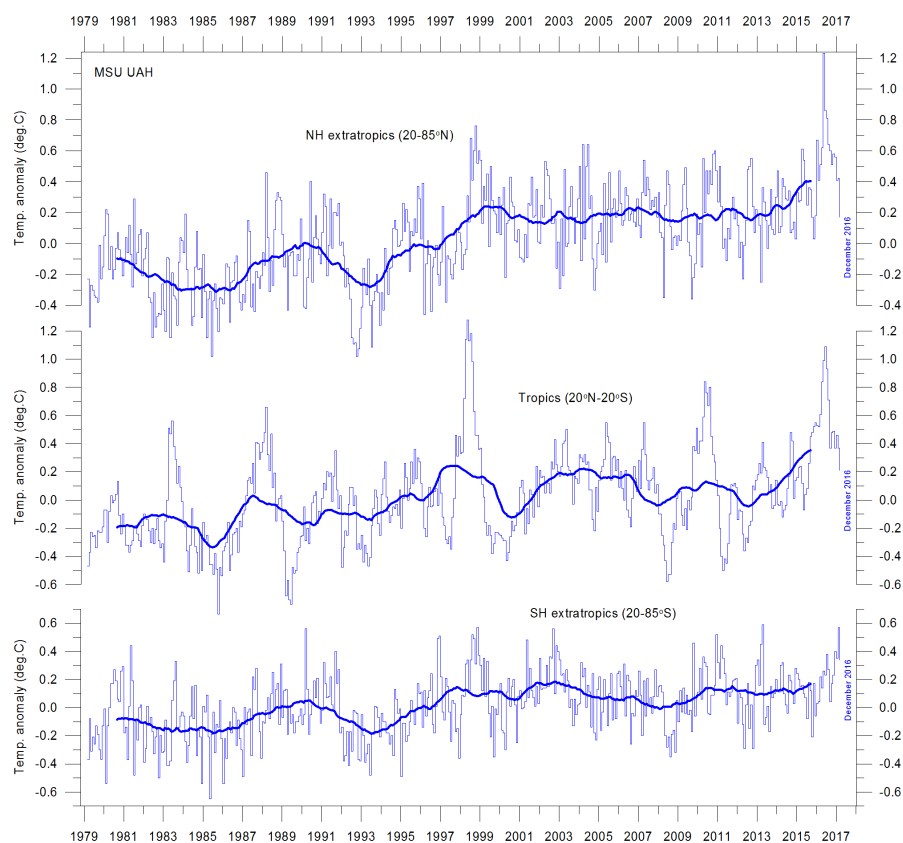


Figure 14: Global monthly average lower troposphere temperature since 1979 for the tropics and the northern and southern extratropics, according to UAH.

Thick lines are the simple running 37-month average, nearly corresponding to a running 3-yr average.

## 12 Polar air temperatures

In the Arctic, warming commenced around 1995, but has slowed somewhat since about 2005 (Figure 15, top). In 2016, however, temperatures peaked for several months, presumably because of oceanic heat given off to the atmosphere during the El Niño of 2015–16 (see also Figure 17), and transported to higher latitudes.

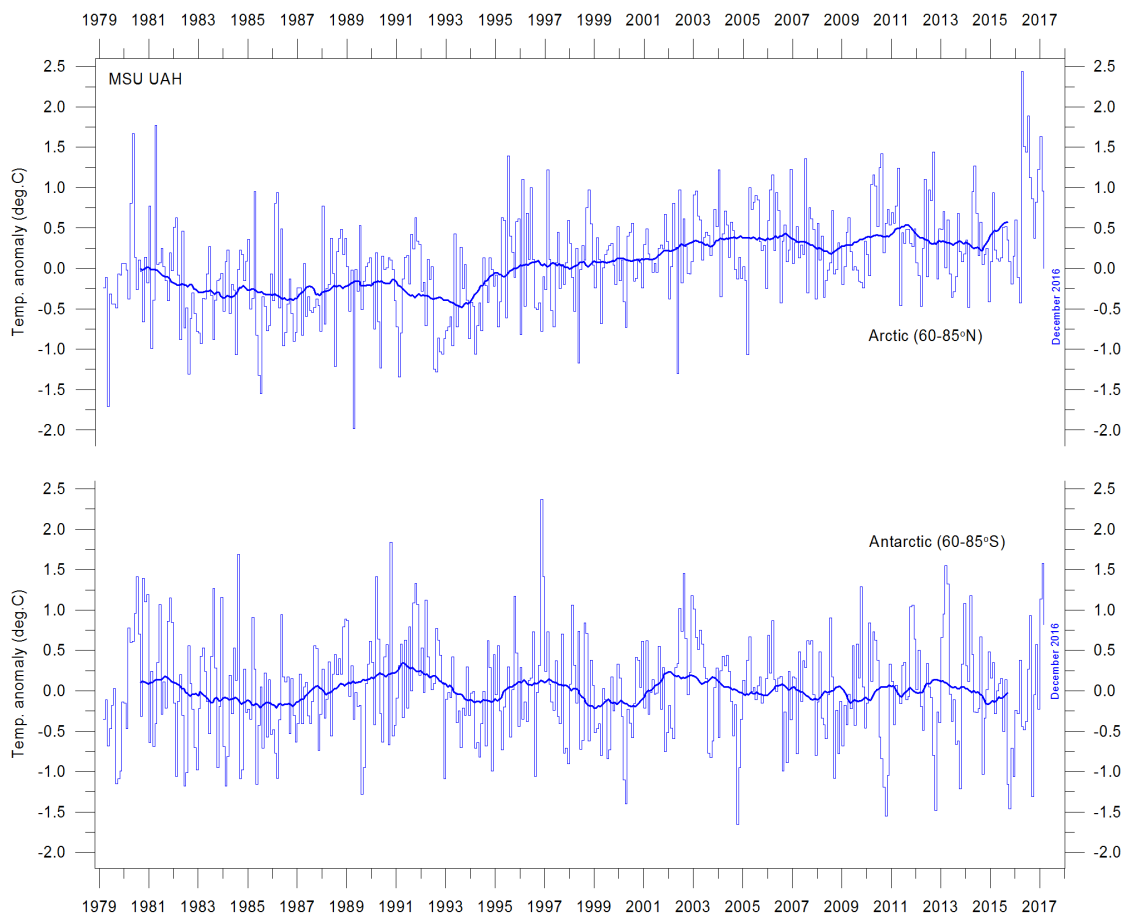


Figure 15: Global monthly average lower troposphere temperature since 1979 for the North Pole and South Pole regions, according to UAH.

Thick lines are the simple running 37-month average, nearly corresponding to a running 3-yr average.

In the Antarctic, temperatures have remained almost stable since the start of the satellite record in 1979 (Figure 15, bottom). In 2016, a small temperature peak is visible in the monthly record and may be interpreted as a subdued effect of the recent El Niño. Much of the additional heat transported to the Arctic following the 2015–16 El

Niño may subsequently have been radiated out to space, according to the ESRL.<sup>†</sup> Latitudes north of 70°N have been characterised by above-normal outgoing longwave radiation during the northern hemisphere fall and early winter of 2016 (Figure 16). In addition, much heat has escaped from the equatorial regions over the Pacific Ocean, corresponding to the area directly affected by the recent El Niño.

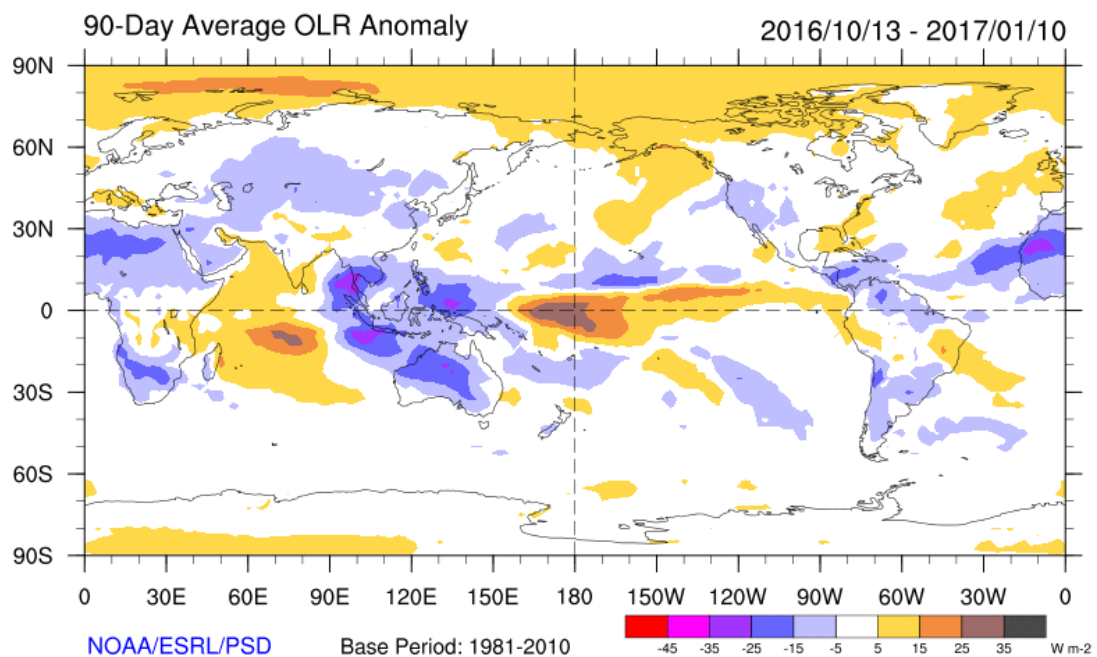


Figure 16: Three-month (13 October 2016–10 January 2017) average outgoing long wave radiation (OLR) anomaly at the top of the atmosphere.

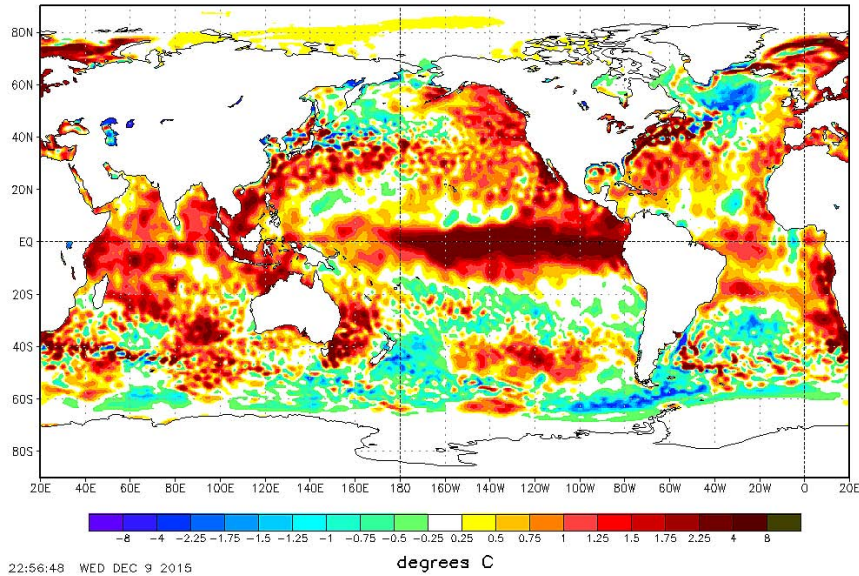
Source: ESRL.

### 13 Sea surface temperature anomaly at the end of 2015 and 2016

Figure 17 shows the recent El Niño in December 2015 (top) compared to the situation in December 2016 (bottom), after the El Niño had come to an end and with the situation moving towards La Niña conditions.

<sup>†</sup> ESRL is the Earth System Research Laboratory at the US National Oceanographic and Atmospheric Administration

NOAA/NWS/NCEP/EMC Marine Modeling and Analysis Branch  
RTG\_SST Anomaly (0.5 deg X 0.5 deg) for 09 Dec 2015



NOAA/NWS/NCEP/EMC Marine Modeling and Analysis Branch  
RTG\_SST Anomaly (0.5 deg X 0.5 deg) for 29 Dec 2016

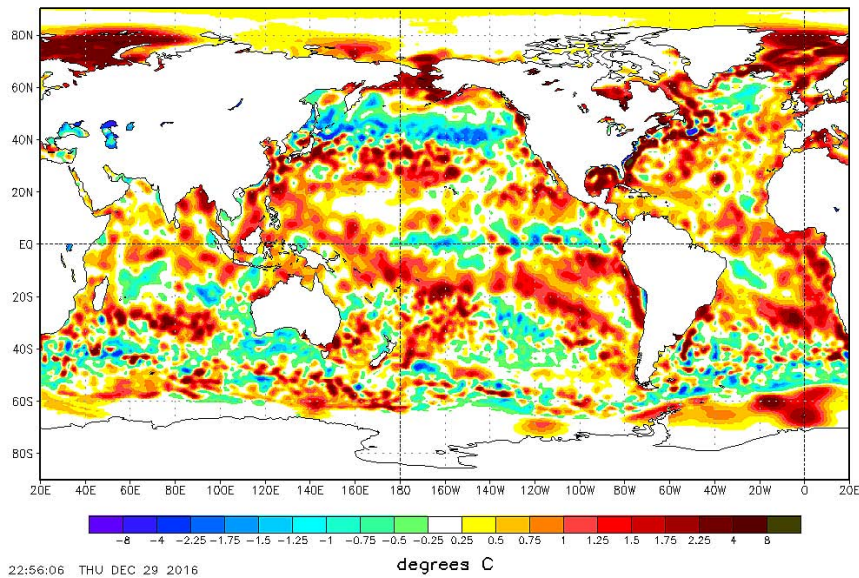


Figure 17: Sea surface temperature anomalies December 2015 and 2016 (°C).

The maps show the current anomaly (deviation from normal) of the surface temperature of Earth's oceans. White areas in the oceans near the poles show the extent of sea ice. Map source: National Centers for Environmental Prediction.

It is also clear from Figure 18 that the 2015–16 El Niño was among the strongest since the beginning of the record in 1950. Considering the entire record, however, recent variations of El Niño and La Niña episodes do not appear abnormal.

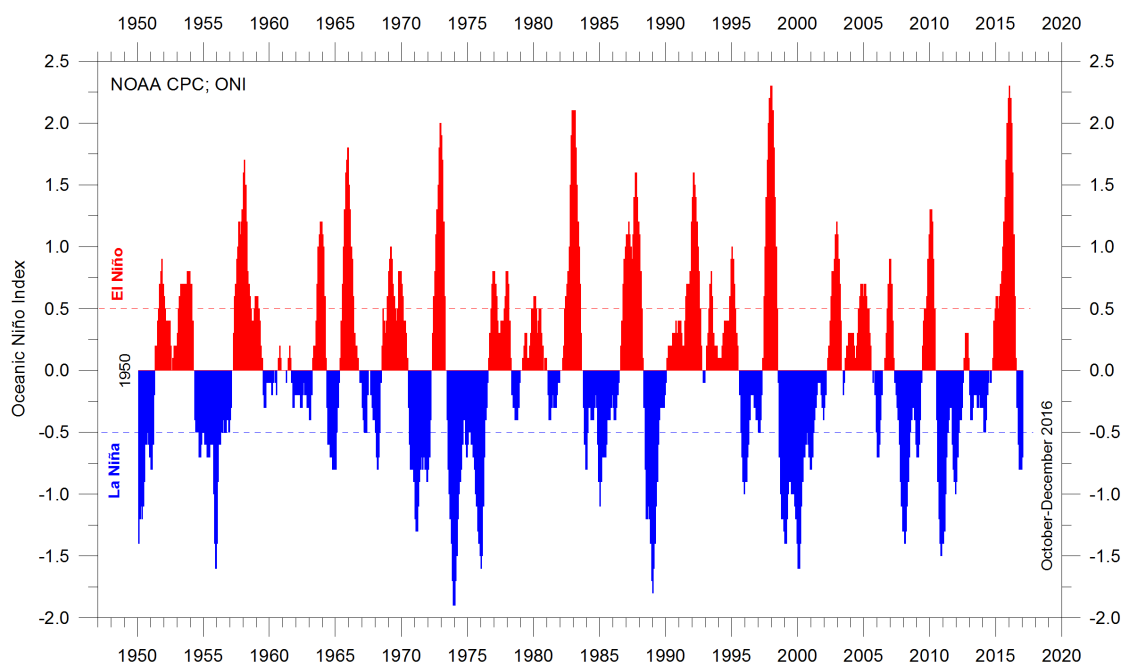


Figure 18: Warm and cold episodes for the Oceanic Niño Index (ONI). The ONI is defined as 3-month running mean of ERSSTv4 SST anomalies in the Niño 3.4 region (5°N-5°S, 120°-170°W). Anomalies are centered on 30-yr base periods updated every 5 years.

## 14 Global ocean average temperatures to 1900 m depth

The global summary in Figure 19 shows that, on average, the temperature of the global oceans down to 1900 m depth has been increasing since about 2008, but not previously. Furthermore, it is seen that this increase is predominantly due to oceanic changes near the Equator, between 30°N and 30°S. Near the Arctic, north of 55°N, ocean temperatures are decreasing. Near the Antarctic, south of 55°S, temperatures are essentially stable. At all latitudes, a clear annual rhythm is seen.

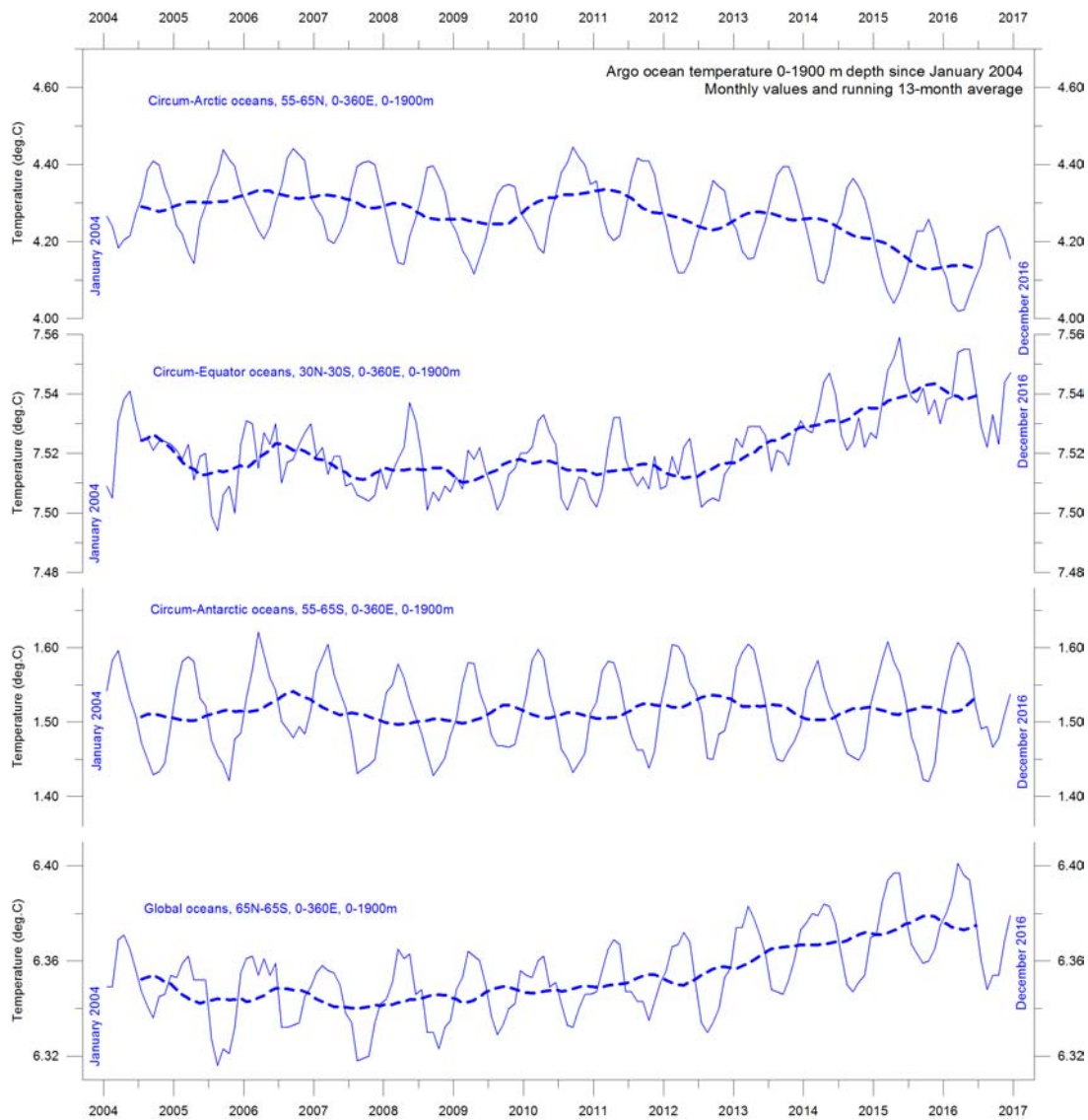


Figure 19: Average ocean temperatures 0–1900 m depth in selected latitudinal bands, using Argo data.

The thin line shows monthly values and the thick line shows the running 13-month average. Source: Global Marine Argo Atlas.

## 15 Global ocean temperatures at different depths

Figure 20 shows global average oceanic temperatures at different depths. The annual rhythm can be observed down to about 100 m depth. In the uppermost 100 m, temperatures have increased since about 2011, while at 200 m depth, temperatures have decreased.

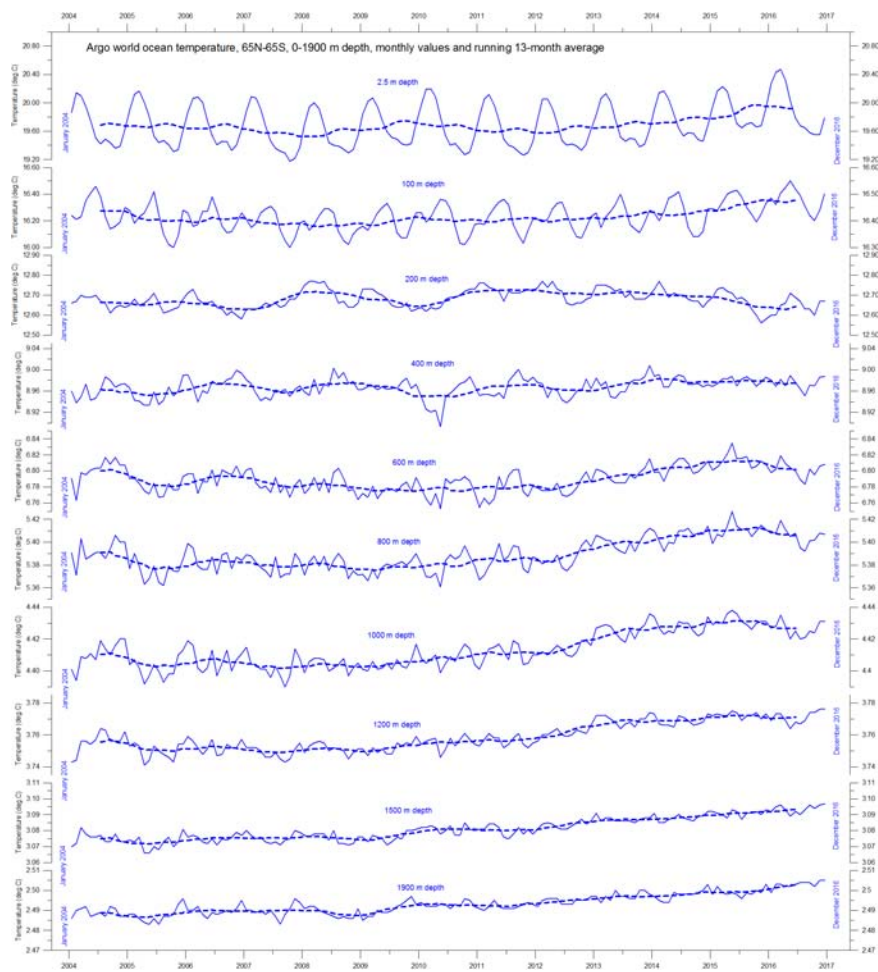


Figure 20: Global ocean temperatures at different depths between 65°N and 65°S, using Argo-data.

The thin line shows monthly values and the thick line shows the running 13-month average. Source: Global Marine Argo Atlas.

Below 400 m, however, temperatures are again seen to be increasing. The diagram suggests that this increase first commenced at 1900 m depth around 2009, and from there has been gradually spreading upwards. At 600 m depth, the present temperature increase began around 2012, about three years later than at 1900 m. Thus, part of the present ocean warming appears to be due to circulation features at depths greater than 1900 m, and not related directly to processes operating at or near the sea surface.

This development is also seen in Figure 21, which shows the net change of ocean temperature at different depths, calculated as the difference between the annual averages for 2004 and 2016.

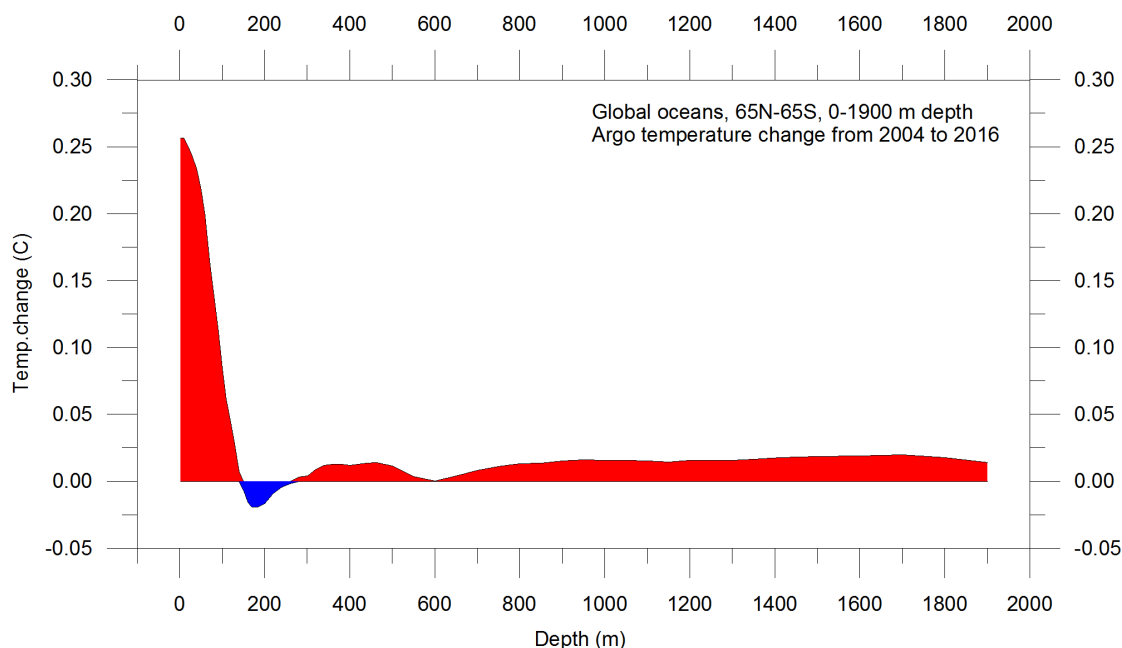


Figure 21: Net change of ocean temperature at different depths.

## 16 Regional ocean temperature changes at 0–1900 m

The maximum surface warming (down to about 120 m) affects oceans near the Equator, and surface warming is absent or small at higher latitudes in both hemispheres. Thus the maximum ocean surface warming has taken place at latitudes where the incoming solar radiation is at its annual maximum.

Cooling is pronounced for the northern oceans. However, the major part of Earth's land areas is in the northern hemisphere, so the surface area (and volume) of 'Arctic' oceans is much smaller than the 'Antarctic' oceans, which is in turn smaller than the 'Equatorial' oceans.

Nevertheless, the contrast in net temperature changes in 2004–2016 for the different latitudinal bands is revealing. For the polar oceans, the data appears to demonstrate the existence of a bi-polar seesaw, as described by Chylek et al. (2010).<sup>†</sup> It is no less interesting that the near-surface ocean temperatures in the two polar regions contrast with the overall development of sea ice in the same regions (see p. 33).

<sup>†</sup> Chylek, P., Folland, C. K., Lesins, G., and Dubey, M. K. 2010. Twentieth century bipolar seesaw of the Arctic and Antarctic surface air temperatures. *Geophysical Research Letters*, 37, L08703, doi:10.1029/2010GL042793.

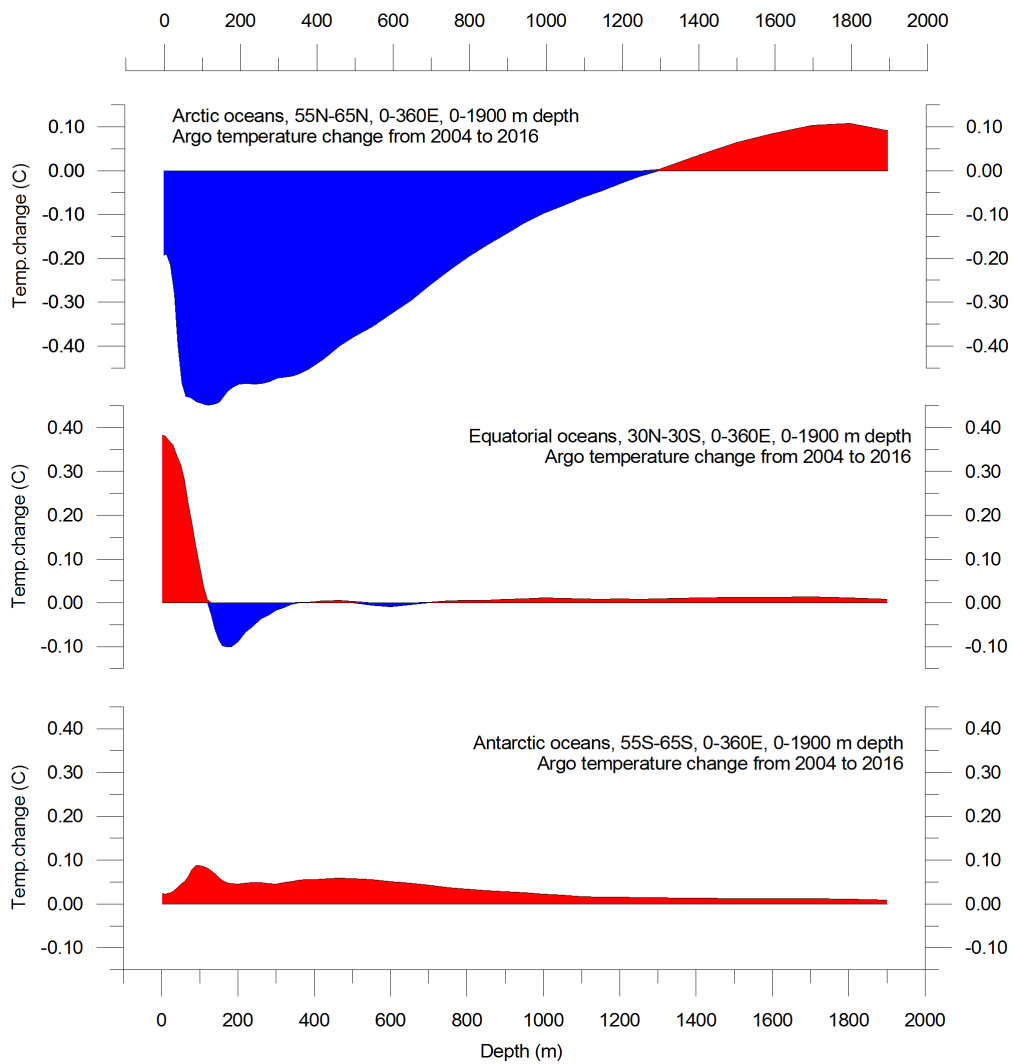


Figure 22: Latitudinal variation of oceanic temperature changes for 2004–2016 at various depths, calculated as per the previous diagram.

The three panels show the change in Arctic oceans (55–65°N), equatorial oceans (30°N–30°S), and Antarctic oceans (55–65°S), respectively.

## 17 Ocean temperature net change 2004–2016 in two north–south sectors

This section examines temperature changes for 2004–2016 along two lines of longitude, representing the Atlantic and the Pacific oceans (see Figure 23). The data come from the Argo floats.

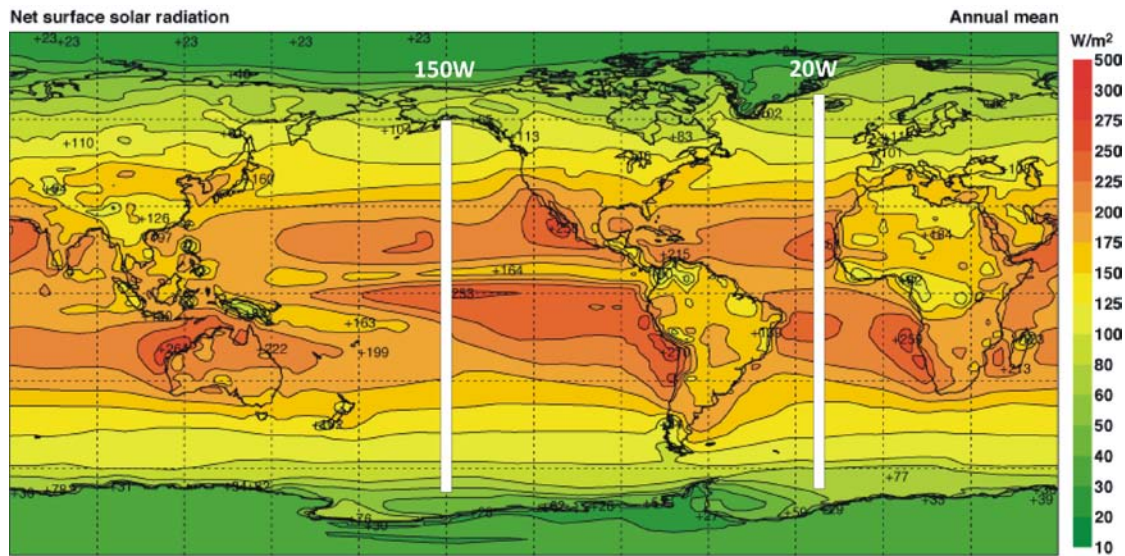


Figure 23: Map showing average annual mean net surface solar radiation ( $\text{W}/\text{m}^2$ ), and the location of two longitudinal profiles, shown below.

The results are shown in Figure 24. To prepare the diagram, annual average temperatures for 2016 were compared to annual average temperatures for 2004, the latter representing the first year in the Argo record. Warm colours indicate net warming from 2004 to 2016, and blue colours cooling. Due to the spherical form of the Earth, northern and southern latitudes represent only small ocean volumes, compared to the latitudes near the Equator.

With this reservation in mind, the Atlantic diagram (Figure 24a) nevertheless reveals some interesting features. The most prominent feature is a marked cooling north of  $30^\circ\text{N}$ , while warming – less pronounced – dominates south of  $20^\circ\text{S}$ , down to depths of 1200 m. The maximum warming is confined to approximately the uppermost 100 m between  $20^\circ\text{N}$  and  $35^\circ\text{S}$ , but especially around  $25\text{--}30^\circ\text{S}$ . Warming has also taken place north of  $30^\circ\text{N}$  at depths greater than 1500 m in the  $20^\circ\text{W}$  profile.

Figure 24b shows the net changes for the Pacific Ocean profile, along  $170^\circ\text{W}$ . Again, northern and southern latitudes represent only relatively small ocean volumes compared to latitudes near the Equator.

The most prominent feature is a marked cooling, near or below the surface, between  $20$  and  $55^\circ\text{S}$ . The maximum warming is confined to the uppermost about 100 m, centred on  $10^\circ\text{N}$  and  $10^\circ\text{S}$ , respectively. In addition, surface warming has also taken place between  $50$  and  $58^\circ\text{N}$ , roughly corresponding to the ‘Pacific Warm Blob’. Slight net warming also characterises water depths down to 1100 m north of the Equator. In the southern hemisphere south of  $30^\circ\text{S}$ , net cooling dominates all water depths down to 1900 m.

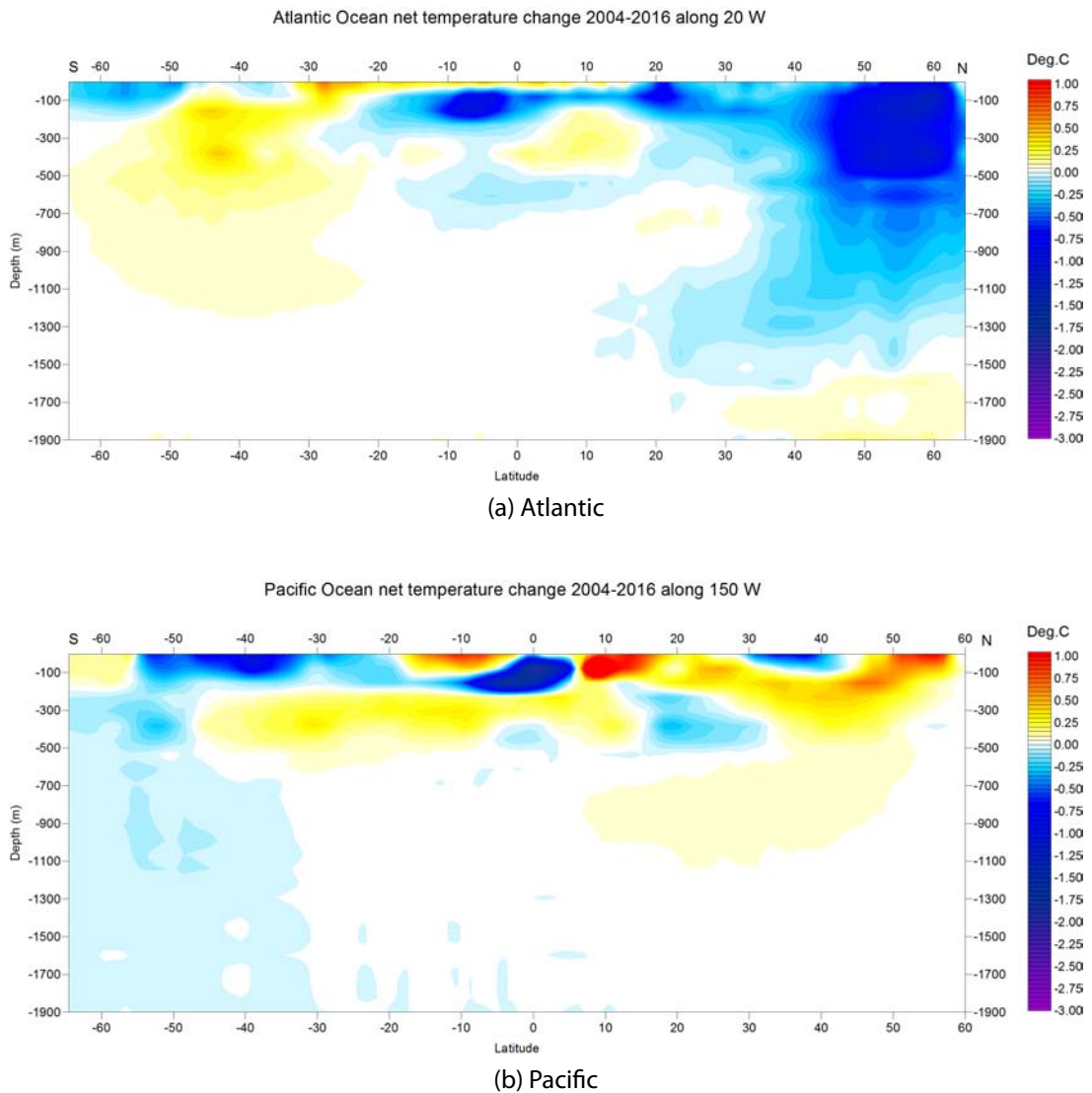
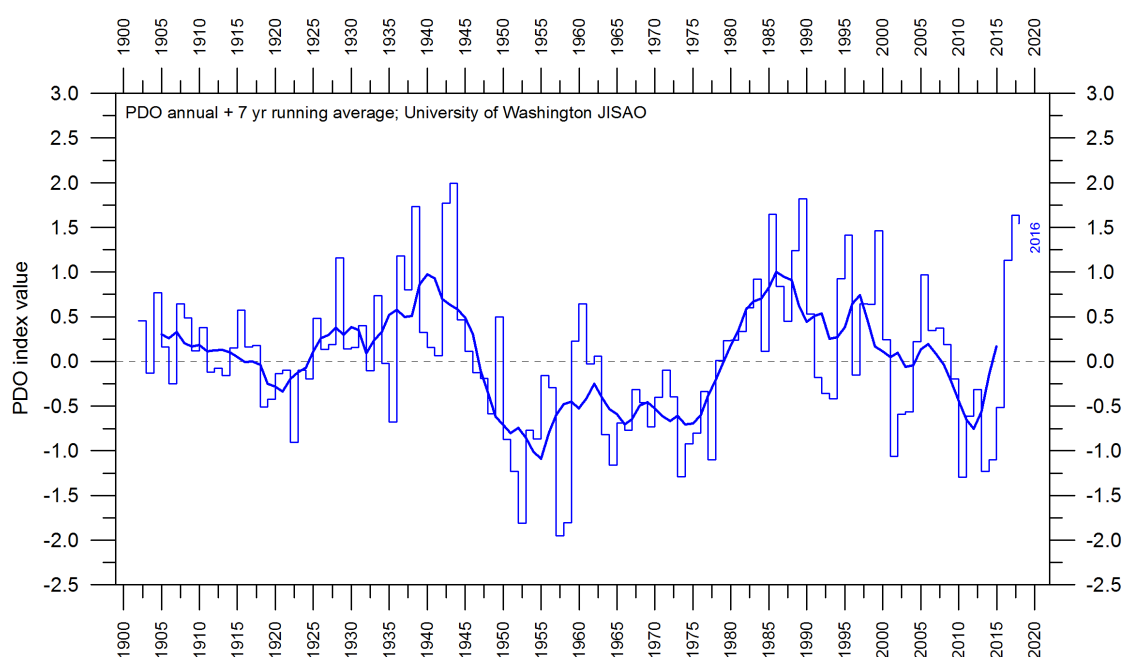


Figure 24: Ocean temperature change along two longitudinal profiles.

Neither part of Figure 24 shows to what extent the net changes shown are caused by ocean dynamics operating east and west of the two profiles considered; they only display net changes for 2004–2016 along the longitude chosen. For that reason, the diagrams should not be overinterpreted. However, the most prominent surface warming in the two profiles generally appears to coincide with the latitudes of maximum net solar radiation (see Figure 23). In addition, the two profiles suggest an interesting contrast, with the Pacific Ocean mainly warming north of Equator, and cooling in the south, while the opposite is happening in the Atlantic profile, with cooling in the north and warming in the south.

## 18 Pacific Decadal Oscillation

The Pacific Decadal Oscillation (PDO) is a long-lived El Niño-like pattern of Pacific climate variability, with data extending back to January 1900. The causes of the PDO are not currently known, but even in the absence of a theoretical understanding, information about it improves season-to-season and year-to-year climate forecasts for North America because it has a strong tendency to multi-season and multi-year persistence. The PDO also appears to be roughly in phase with global temperature changes. Thus, from a societal-impacts perspective, recognition of the PDO is important because it shows that 'normal' climate conditions can vary over time periods comparable to the length of a human lifetime.



**Figure 25: Annual values of the Pacific Decadal Oscillation (PDO)**  
Data from the Joint Institute for the Study of the Atmosphere and Ocean (JISAO), a cooperative institute of the National Oceanic and Atmospheric Administration and the University of Washington, USA. The thin line shows the annual PDO values, and the thick line is the simple running 7-year average.

A Fourier frequency analysis (not shown) shows the PDO record to be influenced by a 5.7-year cycle, and possibly also by a longer cycle of about 53 years' duration.

## 19 Atlantic Multidecadal Oscillation

The Atlantic Multidecadal Oscillation (AMO) is a mode of variability occurring in the North Atlantic surface temperature field. The AMO is basically an index of North Atlantic sea surface temperatures (SST).

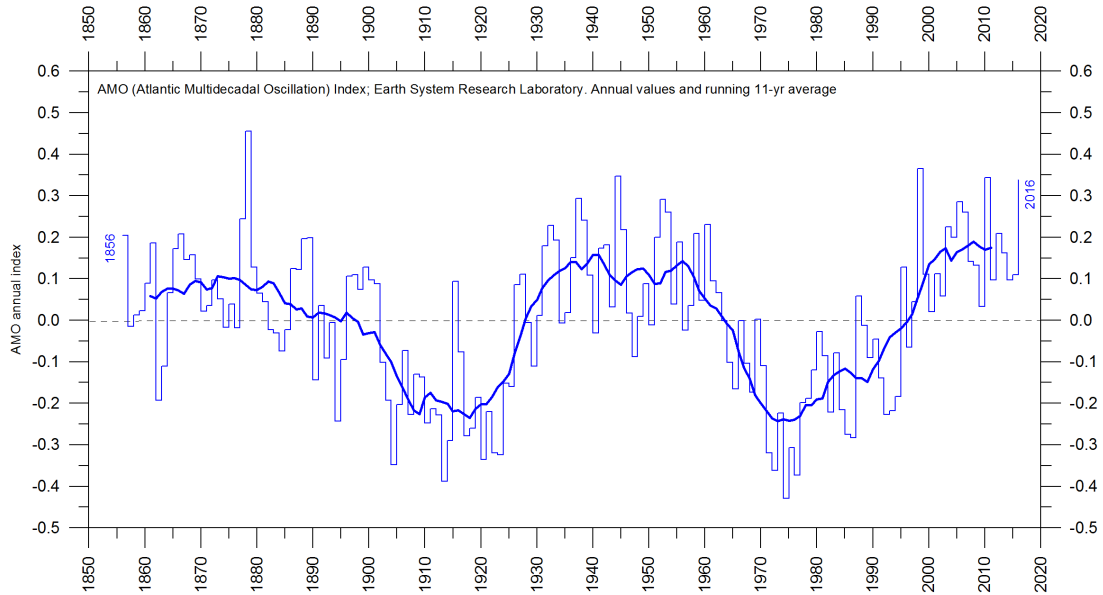


Figure 26: Annual Atlantic Multidecadal Oscillation (AMO) detrended and unsmoothed index values since 1856.

The thin blue line shows annual values, and the thick line is the simple running 11-year average. Data source: Earth System Research Laboratory, NOAA, USA.

The AMO index appears to be correlated to air temperatures and rainfall over much of the northern hemisphere. The association appears to be high for northeastern Brazil, African Sahel rainfall and North American and European summer climate. The AMO index also appears to be associated with changes in the frequency of North American droughts and is reflected in the frequency of severe Atlantic hurricanes.

As one example, the AMO index may be related to the past occurrence of major droughts in the US Midwest and the south-west. When the AMO is high, these droughts tend to be more frequent or prolonged, and less so for low values of AMO. Two of the most severe droughts of the 20th century in the USA – the Dustbowl of the 1930s and the 1950s droughts – occurred during the peak AMO values between 1925 and 1965. On the other hand, Florida and the Pacific north-west tend to be the opposite; a high AMO is here associated with relatively high precipitation.

A Fourier-analysis (not shown here) shows the AMO record to be controlled by a cycle of about 67 years, and to a lesser degree by a 3.5-year cycle.

## 20 Sea level from satellite altimetry

Satellite altimetry is a new and valuable type of measurement, providing a unique insight into the detailed surface topography of the oceans, and its changes. However, it is not a precise tool for estimating changes in global sea level due to a number of assumptions made when interpreting the original satellite data.

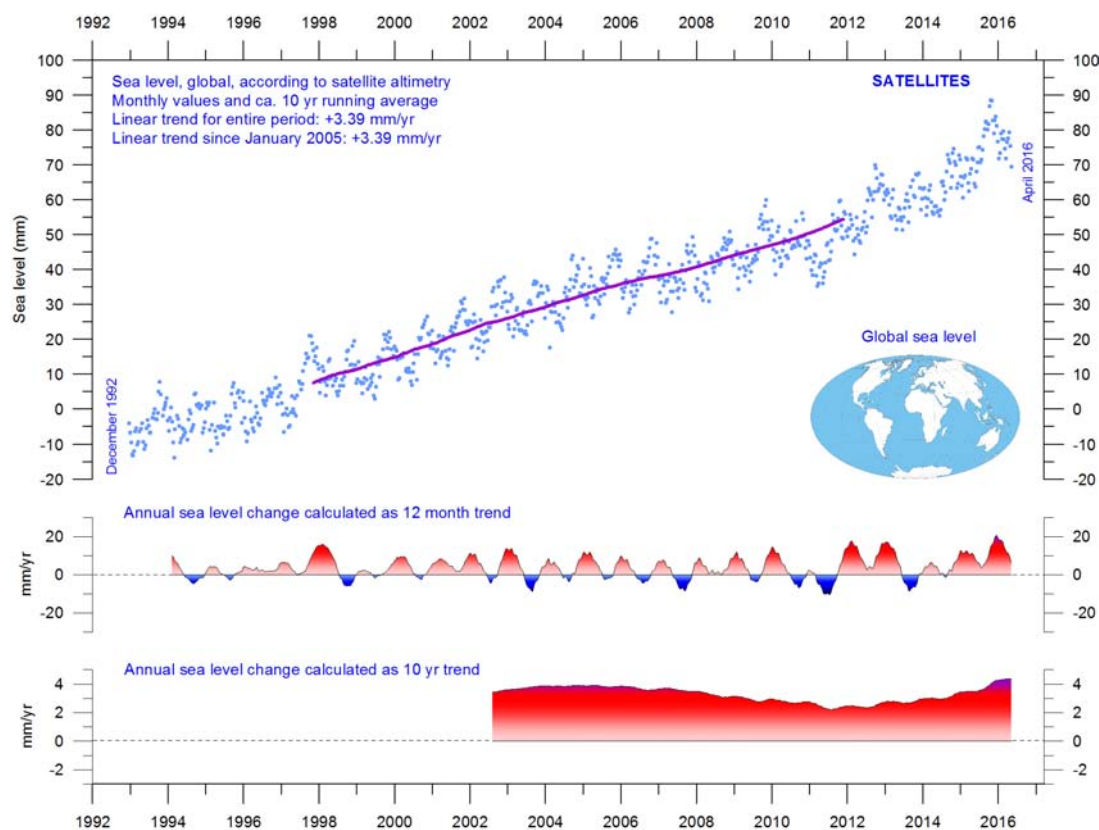


Figure 27: Global sea level since December 1992 according to the Colorado Center for Astroynamics Research at University of Colorado at Boulder.

The blue dots are the individual observations, and the purple line represents the running 121-month ( 10-yr) average. The two lower panels show the annual sea level change, calculated for 1- and 10-yr time windows, respectively. These values are plotted at the end of the interval considered.

One of the assumptions made during the interpretation of satellite altimetry data is the amount of correction required, locally and regionally, to the glacial isostatic adjustment (GIA). The GIA relates to the large-scale, long-term mass transfer from the oceans to the land, in the form of rhythmic waxing and waning of the large Quaternary ice sheets in North America and northern Europe. This enormous mass transfer causes rhythmic changes in surface loads, resulting in a viscoelastic mantle flow and

elastic effects in the upper crust. No single technique or observational network can give enough information on all aspects and consequences of the GIA, so the assumptions adopted for the interpretation of satellite altimetry data are difficult to verify. The GIA correction used in the interpretation of data from satellite altimetry depends on the choice of models used: for the melting of the ice sheets since the last deglaciation and for the crust-mantle. As a consequence of this (and additional factors), interpretations of modern global sea level change based on satellite altimetry vary from about 1.7 mm/yr to about 3.2 mm/yr.

## 21 Sea level from tide gauges

Tide gauges are located at coastal sites, and record the net movement of the local ocean surface in relation to the land. Local relative sea-level change is the important factor for purposes of coastal planning, so tide-gauge data are directly applicable for planning for coastal installations.

In a more scientific context, the measured net movement of the local sea-level is composed of two local components:

- the vertical change of the ocean surface
- the vertical change of the land surface.

For example, a tide gauge may record an apparent sea-level increase of 3 mm/year. If geodetic measurements show the land to be sinking by 2 mm/year, the real sea level rise is only 1 mm/year (3 minus 2 mm/year). In a global sea-level change context, the value of 1 mm/year is relevant, but in a local coastal planning context the 3 mm/year value is more relevant.

To construct time series of sea-level measurements at each tide gauge, the monthly and annual means have to be reduced to a common datum. This reduction is performed by making use of the tide-gauge datum history provided by the supplying authority. The Revised Local Reference (RLR) datum at each station is defined to be approximately 7000 mm below mean sea level, with this arbitrary choice made many years ago in order to avoid negative numbers in the resulting RLR monthly and annual mean values.

Most tide gauges are located at sites exposed to tectonic uplift or sinking (the vertical change of the land surface). This widespread vertical instability has several causes, but of course affects the interpretation of data from the individual tide gauges, although much effort is put into correcting for local tectonic movements.

Of special interest concerning the real short- and long-term sea-level change is therefore data obtained from tide gauges located at tectonically stable sites. One example of such a long record is shown in Figure 29. This record indicates a stable sea-level rise of about 0.84 mm per year, with no indication of recent acceleration.

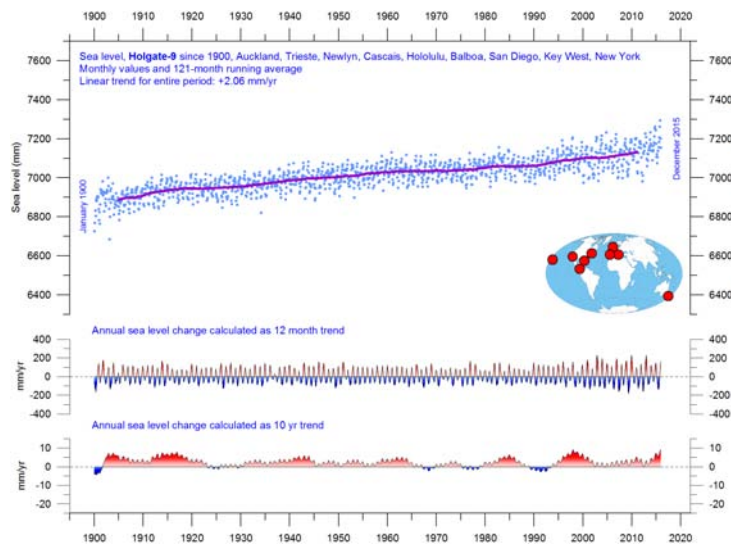


Figure 28: Holgate-9 monthly tide-gauge data.

Holgate (2007) suggested the nine stations listed in the diagram to capture the variability found in a larger number of stations over the last half century studied previously. For that reason, average values of the Holgate-9 group of tide gauge stations are interesting to follow. The blue dots are the individual average monthly observations, and the purple line represents the running 121-month (10-yr) average. The two lower panels show the annual sea-level change, calculated for 1- and 10-yr time windows, respectively. These values are plotted at the end of the interval considered. Source: from PSMSL Data Explorer.

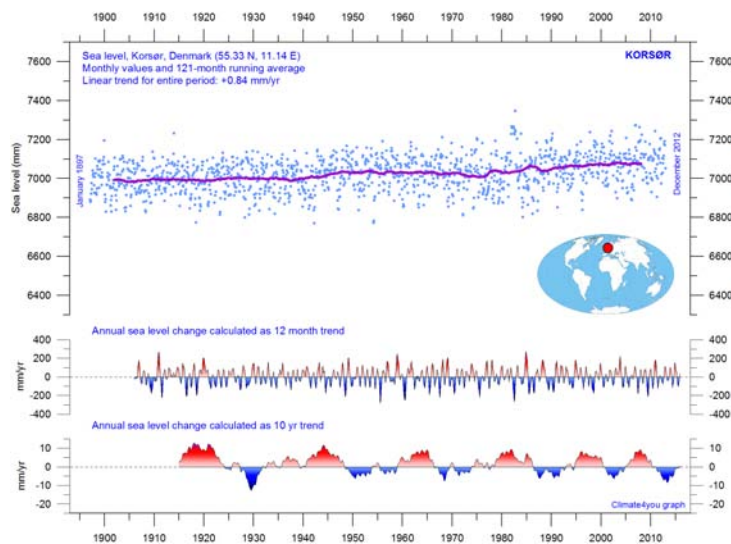


Figure 29: Korsør (Denmark) monthly tide gauge data since January 1897.

The blue dots are the individual monthly observations, and the purple line represents the running 121-month (~10-yr) average. The two lower panels show the annual sea level change, calculated for 1 and 10-yr time windows, respectively. These values are plotted at the end of the interval considered. Source: from PSMSL Data Explorer.

Data from tide gauges all over the world suggest an average global sea-level rise of only 1–1.5 mm/yr, while the satellite-derived record (see above) suggests a rise of more than 3 mm/yr. The noticeable difference between the two data sets has no broadly accepted explanation.

## 22 Annual accumulated cyclone energy for the Atlantic Basin

Accumulated cyclone energy (ACE) is a measure used by the National Oceanic and Atmospheric Administration to express the activity of individual tropical cyclones and entire tropical cyclone seasons. ACE is calculated as the square of the wind speed every 6 h, and is then scaled by a factor of 10,000 for usability, using a unit of  $10^4$  knots<sup>2</sup>. The ACE of a season is the sum of the ACE for each storm, and takes into account the number, strength, and duration of all the tropical storms in the season.

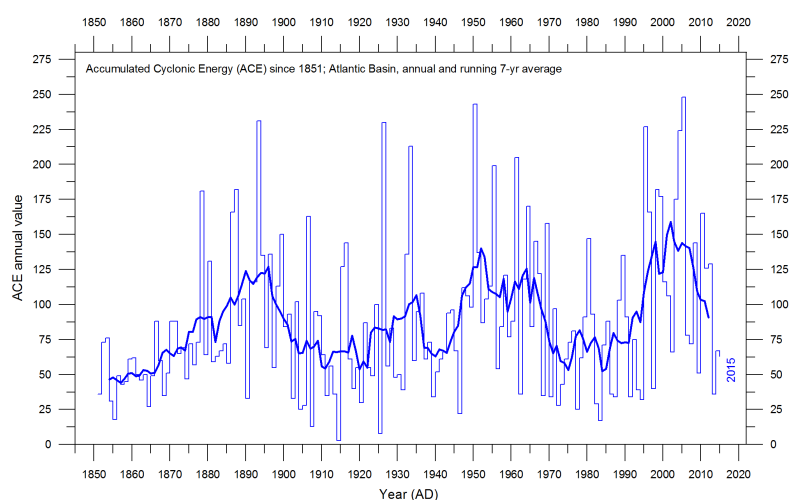


Figure 30: Accumulated cyclone energy for the Atlantic basin per year since 1850 AD.

Thin lines show annual ACE values, and the thick line shows the running 7-yr average.

Data source: Atlantic Oceanographic and Meteorological Laboratory, Hurricane Research Division.

The damage potential of a hurricane is proportional to the square or cube of the maximum wind speed, and thus ACE is not only a measure of tropical cyclone activity, but also a measure of the damage potential of an individual cyclone or a season.

A Fourier analysis of the ACE series for the Atlantic Basin (not shown) reveals it to be strongly influenced by a periodic variation of about 60 years' duration. At present, the ACE series is displaying a declining trend.

## 23 Global, Arctic and Antarctic sea-ice extent

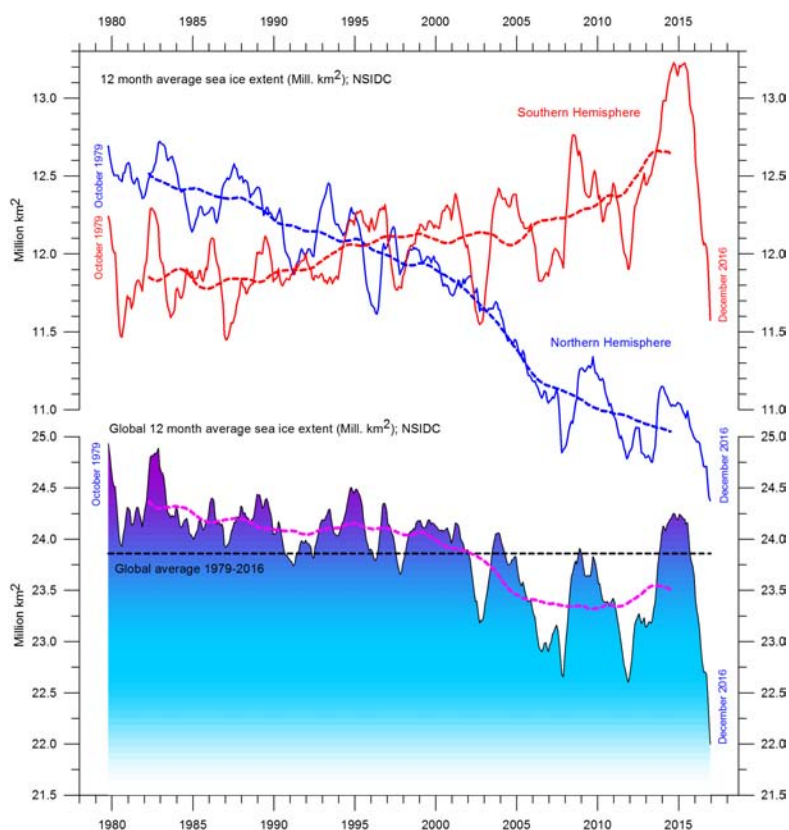


Figure 31: Global and hemispheric 12-month running average sea-ice extent since 1979, the satellite-era.

The October 1979 value represents the monthly average of November 1978–October 1979, the November 1979 value represents the average of December 1978–November 1979, and so on. The stippled lines represent a 61-month ( 5-yr) average. The last month included in the 12-month calculations is shown to the right of the diagram.

Data source: National Snow and Ice Data Center (NSIDC).

The two 12-month average sea-ice extent graphs show opposite trends. The modern northern hemisphere trend is towards smaller sea-ice extent, as clearly displayed by the blue line in Figure 31; the simultaneous increase of southern hemisphere sea-ice extent is similarly clear (red line).

Both 12-month average graphs are characterised by repeated variations superimposed on the overall trends. The Arctic extent is strongly influenced by a 5.3-year periodic variation, while for the Antarctic, a periodic variation of about 4.5 years is important. Both these variations reached their minima simultaneously in 2016, which explains the recent minimum in global sea-ice extent.

Presumably, during the coming 1–2 years these natural variations will again induce an increase in sea-ice extent at both poles, with an increase in the 12-month average global sea-ice extent as the likely result. However, in the coming years minima and maxima for these variations will not occur synchronously because of their different length, and global minima (or maxima) may be less pronounced than in 2016.

## 24 Northern hemisphere snow-cover extent

The northern hemisphere snow-cover extent exhibits large local and regional variations from year to year (Figure 32). However, the overall tendency since 1972 is towards stable northern hemisphere snow conditions, as shown in Figures 33 and 34.

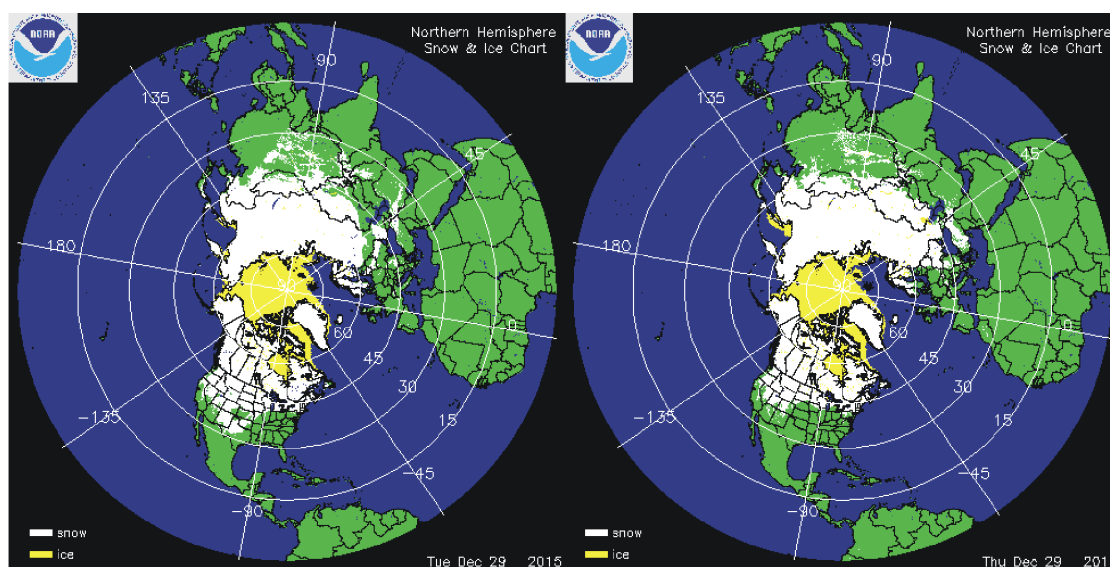


Figure 32: Northern hemisphere snow cover (white) and sea ice (yellow) 29 December 2015 (left) and 2016 (right).

Source: National Ice Center (NIC).

The spring snow cover extent has decreased a little since 1972, and the autumn snow extent has increased a little (Figure 36).

During the northern hemisphere summer, the snow cover usually shrinks to about 2,400,000 km<sup>2</sup> (essentially controlled by the extent of the Greenland ice sheet), and during the northern hemisphere winter it increases to about 50,000,000 km<sup>2</sup>, representing about 33% of planet Earth's total land area.

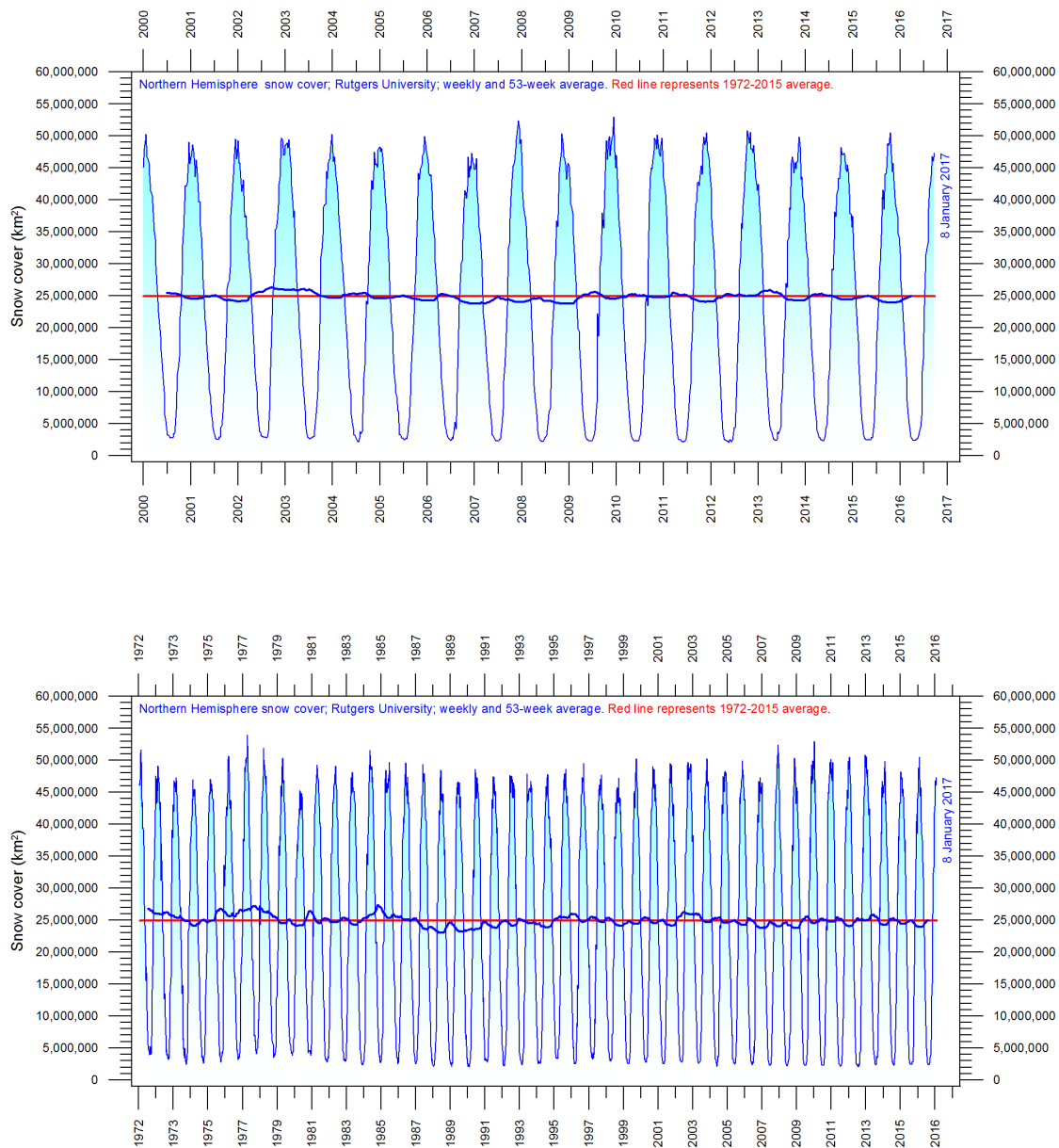


Figure 33: Northern hemisphere weekly snow cover extent since January 2000 (upper diagram) and 1972 (lower diagram).

The thin blue line is the weekly data, and the thick blue line is the running 53-week average ( 1 yr). The horizontal red line is the 1972–2015 average. Source: Rutgers University Global Snow Laboratory.

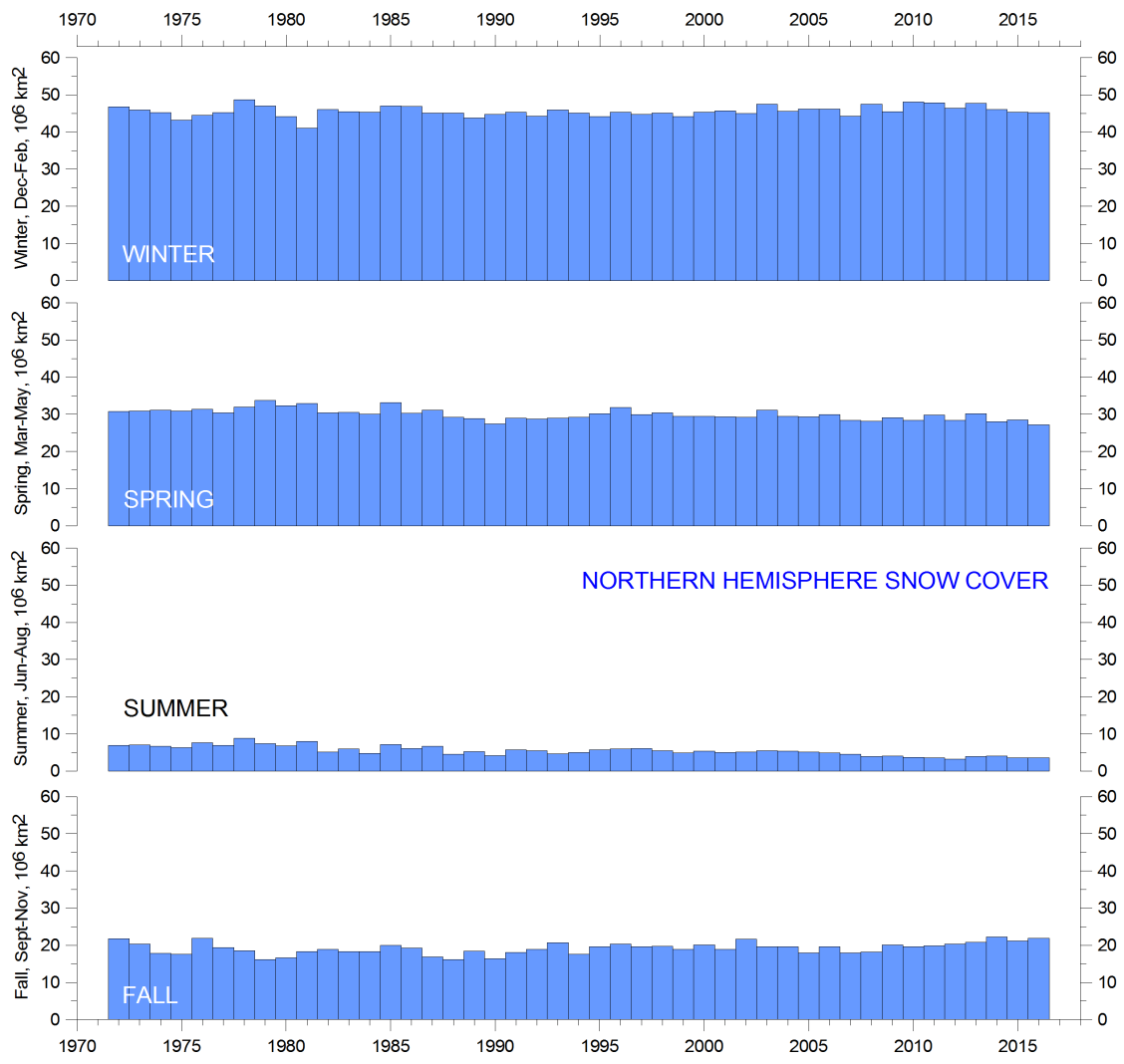


Figure 34: Northern hemisphere seasonal snow cover since 1972.  
 Source: Rutgers University Global Snow Laboratory.

## 25 Links to data sources

AMO, Earth System Research Laboratory, NOAA, USA: <https://www.esrl.noaa.gov/psd/data/timeseries/AMO/>

Atlantic Oceanographic and Meteorological Laboratory, Hurricane Research Division: <http://www.aoml.noaa.gov/hrd/tcfaq/E11.html>

Colorado Center for Astrodynamic Research: <http://sealevel.colorado.edu/>

Earth System Research Laboratory (ESRL): <https://www.esrl.noaa.gov/psd/map/clim/olr.shtml>

GISS temperature data: <https://data.giss.nasa.gov/gistemp/>

Global Marine Argo Atlas: [http://www.argo.ucsd.edu/Marine\\_Atlas.html](http://www.argo.ucsd.edu/Marine_Atlas.html)

Goddard Institute for Space Studies (GISS): <https://www.giss.nasa.gov/>

HadCRUT temperature data: <http://hadobs.metoffice.com/>

National Ice Center (NIC). [http://www.natice.noaa.gov/pub/ims/ims\\_gif/DATA/cursnow.gif](http://www.natice.noaa.gov/pub/ims/ims_gif/DATA/cursnow.gif)

National Snow and Ice Data Center (NSIDC): [http://nsidc.org/data/seaice\\_index/index.html](http://nsidc.org/data/seaice_index/index.html)

NCDC temperature data: <https://www.ncdc.noaa.gov/monitoring-references/faq/>

Ocean temperatures from Argo floats: <http://www.argo.ucsd.edu/>

Oceanic Niño Index (ONI): [http://www.cpc.ncep.noaa.gov/products/analysis\\_monitoring/ensostuff/ensoyears.shtml](http://www.cpc.ncep.noaa.gov/products/analysis_monitoring/ensostuff/ensoyears.shtml)

Outgoing longwave radiation (OLR): <https://www.esrl.noaa.gov/psd/map/clim/olr.shtml>

PDO, Joint Institute for the Study of the Atmosphere and Ocean (JISAO): <http://research.jisao.washington.edu/pdo/PDO.latest>

PSMSL Data Explorer: <http://www.psmsl.org/data/obtaining/map.html>

Rutgers University Global Snow Laboratory: <http://climate.rutgers.edu/snowcover/index.php>

RSS temperature data: <http://www.remss.com/measurements/upper-air-temperature>

Sea level from satellites: [http://sealevel.colorado.edu/files/current/sl\\_global.txt](http://sealevel.colorado.edu/files/current/sl_global.txt)

Sea level from tide gauges: <http://www.psmsl.org/data/obtaining/map.html>

UAH temperature data: [http://www.nsstc.uah.edu/data/msu/v6.0/tlt/uahncdc\\_lt\\_6.0.txt](http://www.nsstc.uah.edu/data/msu/v6.0/tlt/uahncdc_lt_6.0.txt)

## **GWPF REPORTS**

---

1	Montford	The Climategate Inquiries
2	Ridley	The Shale Gas Shock
3	Hughes	The Myth of Green Jobs
4	McKittrick	What Is Wrong With the IPCC?
5	Booker	The BBC and Climate Change
6	Montford	Nullius in Verba: The Royal Society and Climate Change
7	Goklany	Global Warming Policies Might Be Bad for Your Health
8	Hughes	Why Is Wind Power So Expensive?
9	Lilley	What Is Wrong With Stern?
10	Whitehouse	The Global Warming Standstill
11	Khandekar	The Global Warming-Extreme Weather Link
12	Lewis and Crok	Oversensitive
13	Lewis and Crok	A Sensitive Matter
14	Montford and Shade	Climate Control: Brainwashing in Schools
15	De Lange and Carter	Sea-level Change: Living with Uncertainty
16	Montford	Unintended Consequences of Climate Change Policy
17	Lewin	Hubert Lamb and the Transformation of Climate Science
18	Goklany	Carbon Dioxide: The Good News
19	Adams	The Truth About China
20	Laframboise	Peer Review: Why Scepticism is Essential
21	Constable	Energy Intensive Users: Climate Policy Casualties
22	Lilley	£300 Billion: The Cost of the Climate Change Act
23	Humlum	The State of the Climate in 2016

The Global Warming Policy Foundation is an all-party and non-party think tank and a registered educational charity which, while openminded on the contested science of global warming, is deeply concerned about the costs and other implications of many of the policies currently being advocated.

Our main focus is to analyse global warming policies and their economic and other implications. Our aim is to provide the most robust and reliable economic analysis and advice. Above all we seek to inform the media, politicians and the public, in a newsworthy way, on the subject in general and on the misinformation to which they are all too frequently being subjected at the present time.

The key to the success of the GWPF is the trust and credibility that we have earned in the eyes of a growing number of policy makers, journalists and the interested public. The GWPF is funded overwhelmingly by voluntary donations from a number of private individuals and charitable trusts. In order to make clear its complete independence, it does not accept gifts from either energy companies or anyone with a significant interest in an energy company.

**Views expressed in the publications of the Global Warming Policy Foundation are those of the authors, not those of the GWPF, its trustees, its Academic Advisory Council members or its directors.**

Published by the Global Warming Policy Foundation

For further information about GWPF or a print copy of this report, please contact:

The Global Warming Policy Foundation  
55 Tufton Street, London, SW1P 3QL  
T 0207 3406038 M 07553 361717  
[www.thegwpf.org](http://www.thegwpf.org)

Registered in England, No 6962749  
Registered with the Charity Commission, No 1131448

